An avascular tumor growth model based on porous media mechanics and evolving natural states

An avascular tumor growth model based on porous media mechanics and evolving natural states

P Mascheroni[1], M Carfagna[2], A Grillo[2], D P Boso[1], and B A Schrefler*[3]

[1]*Dipartimento di Ingegneria Civile, Edile ed Ambientale, Università di Padova, Via Marzolo 9, 35131 Padova, Italy*
[2]*Dipartimento di Scienze Matematiche, Politecnico di Torino, Corso Duca degli Abruzzi 24, 10124 Torino, Italy*
[3]*Institute for Advanced Study, Technische Universität München, Lichtenbergstraße 2, 85748 Garching bei München, Germany and Houston Methodist Research Institute, 6670 Bertner Ave, Houston, TX 77030, USA*

Abstract

Mechanical factors play a major role in tumor development and response to treatment. This is more evident for tumors grown *in vivo*, where cancer cells interact with the different components of the host tissue. Mathematical models are able to characterize the mechanical response of the tumor and can provide a better understanding of these interactions. In this work, we present a biphasic model for tumor growth based on the mechanics of fluid-saturated porous media. In our model, the porous medium is identified with the tumor cells and the extracellular matrix, and represents the system's solid phase, whereas the interstitial fluid constitutes the liquid

*Electronic address: bernhard.schrefler@dicea.unipd.it; Corresponding author

phase. A nutrient is transported by the fluid phase, thereby supporting the growth of the tumor. The internal reorganization of the tissue in response to mechanical and chemical stimuli is described by enforcing the multiplicative decomposition of the deformation gradient tensor associated with the solid phase motion. In this way, we are able to distinguish the contributions of growth, rearrangement of cellular bonds, and elastic distortion, which occur during tumor evolution. Results are shown for three cases of biological interest, addressing the growth of a tumor spheroid in the culture medium (i), and the evolution of an avascular tumor growing first in a soft host tissue (ii), and then in a three-dimensional heterogeneous region (iii). We analyze the dependence of tumor development on the mechanical environment, with particular focus on cell reorganization and its role in stress relaxation.

Keywords

Biphasic systems, Porous media, Tumor growth, Remodeling, Cell reorganization, Stress relaxation, Nutrient transport

1 Introduction

At the present time, a unifying description of cancer is lacking. This happens because there exist many tumors characterized by different origins and features, and the determinants of tumor progression are still partially unclear [1]. Cells in solid tumors live in a rich environment, filled with water and macromolecules [2, 3]. Among the latter there are nutrients, used by the cells to survive and duplicate, and several

chemical factors. In particular, growth promoting factors, growth inhibitory factors and chemotactic factors are able to trigger subcellular pathways, which result in different cell behaviors. The extracellular space is also filled by a network of cross-linked proteins, known as the extracellular matrix (ECM). This matrix constitutes a biological scaffold that provides structural and biochemical support to the surrounding cells. By exerting forces on the proteins of the network, cells can migrate towards different regions of the tissue, or proliferate, once they have formed stable bonds. The ECM is also subjected to continuous remodeling by cells, as some of them produce matrix degrading enzymes while others secrete new filaments. Remarkably, all these phenomena are influenced by the mechanical stress to which the tissue is subjected, through mechanisms that are still an active area of research [4, 5, 6, 7]. Cell duplication depends on the balance between biochemical and mechanical inputs, too. While the dependence of cell growth on certain nutrients and growth factors is well documented (see for example [8, 9]), several new studies have been focused on determining the influence of mechanical stress on cell behavior [10, 11]. In one of the first works about this subject, Helmlinger and coworkers [12] showed that a compressive stress was able to inhibit the proliferation of cells in tumor spheroids. These findings were confirmed and extended by later works from the same group [13] and by other researches that used different experimental methodologies [14, 15]. All these phenomena constitute a complex framework, which is continuously enriched by new discoveries and increasingly large data sets. Recently, Hanahan and Weinberg [16, 17] published two landmark papers where they summarize the characteristics shared by malignant tumors. In general, these common traits are related

to the occurrence of a failure in cell control mechanisms, and lead to uncontrolled cell proliferation and avoidance of self-death signaling.

Given all these premises, the problem of describing cancer through mathematical models seems thus very complex, even though such models may give some insight into the understanding of the illness. Several models in the literature focus on the biochemical events occurring during the growth of a tumor. These are generally formulated in terms of balance laws along with advection-diffusion-reaction equations for modeling the evolution of nutrients and suitable closure conditions for the cell velocity field [18]. More recently, mathematical models have considered the mechanical aspects of tumor growth, including the dependence of cell growth and death on compression, the effect of mechanical stresses on the tissues surrounding the tumor, and the constitutive laws connecting stresses and deformations in the tumor tissue [19]. Several models describe the tumor mass as a fluid, which in some cases might be a strong simplification. However, significant theoretical difficulties may arise when modeling tumors as solids. In fact, tumor cells duplicate and die, the ECM remodels continuously, and the ensemble of cells is subjected to internal reorganization and change in adhesion properties. It is difficult to define a reference configuration from which deformations can be calculated, since the material is continuously changing. A possible solution to this problem is found by applying the theory of evolving natural configurations. As the basic concept had its roots in the works of Skalak and Rodriguez [20, 21] (taking in turn inspiration from classical theories in elastoplasticity [22, 23, 24]), Rajagopal and Humphrey [25] applied this theory to describe the growth and remodeling of different tissues. They split the evo-

lution of the system in growth, plastic remodeling, and elastic distortions through a multiplicative decomposition of the deformation gradient tensor. Starting from the early works of Ambrosi and Mollica [26, 27], considering a purely elastic monophasic model to evaluate residual stresses in tumor spheroids, Ambrosi and Preziosi in [28] developed a multiphase framework where internal cell reorganization was also taken into account. In a following work [29], these authors employed the latter model to describe the mechanical properties of concentrated cell suspensions. Model predictions were compared with five experimental tests, providing good agreement with the data. The flow rule for cell bond reorganization was further employed by Giverso and Preziosi [30, 31] to describe experiments of cell aggregate compression. Giverso and coworkers have then summarized the previous findings in a recent work [32], in which a linear approximation was enforced for the elastic distortions in the tumor. In addition, a dimensional analysis of the governing equations was carried out, allowing to decouple the equations describing growth from those related to interstitial fluid flow.

In this work, we extend this modeling framework by including the effect of a nutrient on the tumor growth dynamics. Two cell populations are also taken into account, describing proliferating and necrotic tumor cells. Moreover, we test the influence of external healthy tissues with different mechanical properties on tumor development. These new features are studied for three cases of biological interest, namely the growth of a tumor spheroid in the culture medium, in a soft host tissue and in a three-dimensional heterogeneous environment. The dependence of tumor development on the external mechanical environment is analyzed, with particular

attention on cell reorganization and its impact on stress relaxation.

The paper is then organized as follows: In section 2, we introduce the mathematical model, with a focus on the decomposition of the deformation gradient tensor. In section 3, we describe in detail the simulated benchmark tests. In section 4, we present the numerical results for the three considered growth conditions. Finally, we draw our conclusions and propose further research in section 5.

2 Mathematical model

In our model, a tumor mass is described as a biphasic system comprising a solid and a fluid phase. The solid phase (s) is assumed to consist of cells and ECM. These constitute a scaffold that will be described as a solid medium in the sequel. The fluid phase (f) is identified with the tumor's interstitial fluid. We hypothesize that only two types of cells are relevant for our purposes: the proliferating cells (p) and the necrotic cells (n). In the following, we assume that cells and ECM move with the same velocity. Moreover, we consider only the mass exchange processes involving the fluid phase and the cell populations mentioned above. This leads to another simplifying assumption: In fact, we do not account for ECM explicitly in our model. Rather, from here on, when we speak of "proliferating cells" or "necrotic cells", we actually mean a mixture constituted by the considered type of cells and by the ECM, which, thus, does not take part explicitly to the dynamics of the system under study. The fluid phase comprises a nutrient (N) and another constituent, which we call "water" (W). Clearly, many other chemicals are present in this fluid constituent, even though they are not explicitly accounted for here. In some tests

studied in this work, we shall also consider the presence of a soft host tissue and of a stiff host tissue (e.g., bone), which surround the growing tumor. In our model, we shall assume that these tissues occupy three different subdomains of the same region of space, and that both the soft and the stiff host tissue comprise a solid and a fluid phase, which, in analogy with the notation used for the tumor, are associated with the apices (s) and (f). Again, we use (N) and (W) for identifying the nutrient and the water constituents of the fluid in the soft and stiff host tissue.

2.1 Balance equations

We indicate by K_t the region of space occupied by the system at time t, and we assume that K_t is partitioned into three disjoint sets, i.e., $K_t = \mathcal{T}_t \sqcup \mathcal{H}_t \sqcup \mathcal{B}_t$. Here, $\mathcal{T}_t$ represents the *tumor tissue*, $\mathcal{H}_t$ is a *soft host tissue*, and $\mathcal{B}_t$ denotes a *stiff host tissue*, e.g., the bone. Since the majority of the processes, such as growth and mass exchange among the system's constituents, take place in the tumor we start our discussion by considering only the balance laws holding in the interior of $\mathcal{T}_t$.

Within $\mathcal{T}_t$, we assume that the pore space of the cellular scaffold, which represents the solid phase, is completely filled with the fluid. The system is thus constrained by the saturation condition

$$\varphi^{\mathrm{f}} + \varphi^{\mathrm{s}} = 1, \tag{1}$$

where φ^{α} is the volume fraction of the αth phase ($\alpha = \mathrm{f}, \mathrm{s}$). The different constituents (or species) in the phases are described through their mass fraction ω^{β}, with $\beta = \mathrm{p}, \mathrm{n}$ in the solid phase, and $\beta = \mathrm{N}, \mathrm{W}$ in the fluid phase. The mass balance laws for the constituents of the solid phase (i.e., the proliferating and necrotic cells)

are given by

$$\partial_t \left(\varphi^{\mathrm{s}} \rho^{\mathrm{s}} \omega^{\mathrm{p}}\right) + \operatorname{div}\left(\varphi^{\mathrm{s}} \rho^{\mathrm{s}} \omega^{\mathrm{p}} \boldsymbol{v}^{\mathrm{s}}\right) = \Gamma^{\mathrm{p}}_{\mathrm{p}\to\mathrm{n}} + \Gamma^{\mathrm{p}}_{\mathrm{f}\to\mathrm{p}}, \tag{2}$$

$$\partial_t \left(\varphi^{\mathrm{s}} \rho^{\mathrm{s}} \omega^{\mathrm{n}}\right) + \operatorname{div}\left(\varphi^{\mathrm{s}} \rho^{\mathrm{s}} \omega^{\mathrm{n}} \boldsymbol{v}^{\mathrm{s}}\right) = \Gamma^{\mathrm{n}}_{\mathrm{p}\to\mathrm{n}} + \Gamma^{\mathrm{n}}_{\mathrm{n}\to\mathrm{f}}. \tag{3}$$

Here, ρ^{s} and $\boldsymbol{v}^{\mathrm{s}}$ denote the mass density and the velocity of the solid phase, respectively. The terms $\Gamma^{\mathrm{p}}_{\mathrm{p}\to\mathrm{n}}$, $\Gamma^{\mathrm{p}}_{\mathrm{f}\to\mathrm{p}}$, $\Gamma^{\mathrm{n}}_{\mathrm{p}\to\mathrm{n}}$, and $\Gamma^{\mathrm{n}}_{\mathrm{n}\to\mathrm{f}}$ are sources and sinks of mass that account for the mass exchange processes among the constituents of the system under study. More specifically, $\Gamma^{\mathrm{p}}_{\mathrm{p}\to\mathrm{n}}$ is the rate at which proliferating cells become necrotic, and $\Gamma^{\mathrm{p}}_{\mathrm{f}\to\mathrm{p}}$ is the mass uptake of the proliferating cells due to the exchange of mass with the fluid phase. Analogously, $\Gamma^{\mathrm{n}}_{\mathrm{p}\to\mathrm{n}}$ is the increase of mass of the necrotic cells at the expenses of the proliferating ones, and $\Gamma^{\mathrm{n}}_{\mathrm{n}\to\mathrm{f}}$ denotes the rate at which necrotic cells dissolve in the fluid phase. Summing together (2) and (3), and recalling the constraint on the mass fractions, $\omega^{\mathrm{p}} + \omega^{\mathrm{n}} = 1$, we determine the mass balance law for the solid phase as a whole, i.e.,

$$\partial_t \left(\varphi^{\mathrm{s}} \rho^{\mathrm{s}}\right) + \operatorname{div}\left(\varphi^{\mathrm{s}} \rho^{\mathrm{s}} \boldsymbol{v}^{\mathrm{s}}\right) = \Gamma^{\mathrm{s}}, \tag{4}$$

where Γ_{s} is given by

$$\Gamma^{\mathrm{s}} = \Gamma^{\mathrm{p}}_{\mathrm{p}\to\mathrm{n}} + \Gamma^{\mathrm{p}}_{\mathrm{f}\to\mathrm{p}} + \Gamma^{\mathrm{n}}_{\mathrm{p}\to\mathrm{n}} + \Gamma^{\mathrm{n}}_{\mathrm{n}\to\mathrm{f}}. \tag{5}$$

In particular, we choose $\Gamma^{\mathrm{p}}_{\mathrm{p}\to\mathrm{n}}$ and $\Gamma^{\mathrm{n}}_{\mathrm{p}\to\mathrm{n}}$ such that they balance each other, i.e.,

$$\Gamma^{\mathrm{p}}_{\mathrm{p}\to\mathrm{n}} + \Gamma^{\mathrm{n}}_{\mathrm{p}\to\mathrm{n}} = 0 \quad \Rightarrow \quad \Gamma^{\mathrm{p}}_{\mathrm{p}\to\mathrm{n}} = -\Gamma^{\mathrm{n}}_{\mathrm{p}\to\mathrm{n}}, \tag{6}$$

which implies the equality

$$\Gamma^{\mathrm{s}} = \Gamma^{\mathrm{p}}_{\mathrm{f}\to\mathrm{p}} + \Gamma^{\mathrm{n}}_{\mathrm{n}\to\mathrm{f}}. \tag{7}$$

In addition to (2) and (3) we consider also the mass balance law of the fluid phase as a whole and of the nutrient, i.e.,

$$\partial_t \left(\varphi^{\mathrm{f}}\rho^{\mathrm{f}}\right) + \operatorname{div}\left(\varphi^{\mathrm{f}}\rho^{\mathrm{f}}\boldsymbol{v}^{\mathrm{f}}\right) = \Gamma^{\mathrm{f}}, \tag{8}$$

$$\partial_t \left(\varphi^{\mathrm{f}}\rho^{\mathrm{f}}\omega^{\mathrm{N}}\right) + \operatorname{div}\left(\varphi^{\mathrm{f}}\rho^{\mathrm{f}}\omega^{\mathrm{N}}\boldsymbol{v}^{\mathrm{f}}\right) + \operatorname{div}\boldsymbol{J}^{\mathrm{N}} = \Gamma^{\mathrm{N}}_{\mathrm{N}\to\mathrm{p}} \tag{9}$$

where ρ^{f} and $\boldsymbol{v}^{\mathrm{f}}$ are the mass density and the velocity of the fluid phase, respectively, ω^{N} is the mass fraction of the nutrient, and $\boldsymbol{J}^{\mathrm{N}}$ is the mass flux vector of the nutrient, which is generated by the difference between its own velocity and $\boldsymbol{v}^{\mathrm{f}}$. In this work, we assume that $\boldsymbol{J}^{\mathrm{N}}$ obeys standard Fick's law, which yields the expression $\boldsymbol{J}^{\mathrm{N}} = -\varphi^{\mathrm{f}}\rho^{\mathrm{f}}\boldsymbol{D}^{\mathrm{N}}\operatorname{grad}\omega^{\mathrm{N}}$, where $\boldsymbol{D}^{\mathrm{N}}$ is the diffusion tensor. Finally, Γ^{f} is the rate at which the fluid phase exchanges mass with the solid phase, and $\Gamma^{\mathrm{N}}_{\mathrm{N}\to\mathrm{p}}$ is the term describing the uptake of nutrients from the interstitial fluid to the proliferating cells. Since the biphasic system under study is assumed to be closed with respect to mass, Γ^{s} and Γ^{f} must satisfy the condition

$$\Gamma^{\mathrm{f}} + \Gamma^{\mathrm{s}} = 0, \quad \Rightarrow \quad \Gamma^{\mathrm{s}} = -\Gamma^{\mathrm{f}}. \tag{10}$$

In addition to the mass balance laws (2), (3), (8), and (9), we also consider the momentum balance laws associated with the solid and the fluid phase. By neglecting all external body forces, such as gravity, and accounting for the fact that inertial forces are not relevant in the phenomena considered in this work (indeed, the velocities of both the fluid and the solid phase are very small and vary of a quite slow time scale) the local form of these balance laws can be written as

$$\mathrm{div}\boldsymbol{\sigma}^{\mathrm{s}} + \boldsymbol{m}^{\mathrm{s}} = \mathbf{0}, \tag{11}$$

$$\mathrm{div}\boldsymbol{\sigma}^{\mathrm{f}} + \boldsymbol{m}^{\mathrm{f}} = \mathbf{0}. \tag{12}$$

Moreover, we assume that the system is closed with respect to momentum and, by neglecting the momentum exchange rates related to the mass transfer between the fluid and the solid phase, we express the closure condition as

$$\boldsymbol{m}^{\mathrm{s}} + \boldsymbol{m}^{\mathrm{f}} = \mathbf{0}. \tag{13}$$

Finally, adding together (11) and (12) leads to the balance law of momentum for the system as a whole, i.e.,

$$\mathrm{div}(\boldsymbol{\sigma}^{\mathrm{s}} + \boldsymbol{\sigma}^{\mathrm{f}}) = \mathbf{0}. \tag{14}$$

Equations (1)–(14) must be studied in conjunction with the balance laws pertaining to the subdomains $\mathcal{H}_t$ and $\mathcal{B}_t$.

The saturation constraint applies also in each of the subdomains $\mathcal{H}_t$ and $\mathcal{B}_t$, i.e.,

it holds that

$$\varphi^{\mathrm{s}} + \varphi^{\mathrm{f}} = 1, \qquad \text{in } \mathcal{H}_t \sqcup \mathcal{B}_t. \tag{15}$$

Moreover, since in this work it is assumed that in $\mathcal{H}_t$ and $\mathcal{B}_t$ cells do not proliferate or die, it is sufficient to consider only one mass balance law for the solid phase as a whole, in which neither mass sources nor mass sinks appear. Thus, the mass balance law (4) becomes

$$\partial_t \left(\varphi^{\mathrm{s}} \rho^{\mathrm{s}}\right) + \operatorname{div}\left(\varphi^{\mathrm{s}} \rho^{\mathrm{s}} \boldsymbol{v}^{\mathrm{s}}\right) = 0, \qquad \text{in } \mathcal{H}_t \sqcup \mathcal{B}_t. \tag{16}$$

In addition, the mass balance law for the fluid phase as a whole and for the nutrient read

$$\partial_t \left(\varphi^{\mathrm{f}} \rho^{\mathrm{f}}\right) + \operatorname{div}\left(\varphi^{\mathrm{f}} \rho^{\mathrm{f}} \boldsymbol{v}^{\mathrm{f}}\right) = 0, \qquad \text{in } \mathcal{H}_t \sqcup \mathcal{B}_t, \tag{17}$$

$$\partial_t \left(\varphi^{\mathrm{f}} \rho^{\mathrm{f}} \omega^{\mathrm{N}}\right) + \operatorname{div}\left(\varphi^{\mathrm{f}} \rho^{\mathrm{f}} \omega^{\mathrm{N}} \boldsymbol{v}^{\mathrm{f}}\right) + \operatorname{div} \boldsymbol{J}^{\mathrm{N}} = 0, \qquad \text{in } \mathcal{H}_t \sqcup \mathcal{B}_t. \tag{18}$$

Finally, similarly to (11)–(14), also in this case the linear momentum balance laws and the closure condition $\boldsymbol{m}^{\mathrm{s}} + \boldsymbol{m}^{\mathrm{f}} = \mathbf{0}$ must apply, i.e.,

$$\operatorname{div}(\boldsymbol{\sigma}^{\mathrm{s}} + \boldsymbol{\sigma}^{\mathrm{f}}) = \mathbf{0}, \qquad \text{in } \mathcal{H}_t \sqcup \mathcal{B}_t \tag{19}$$

$$\operatorname{div} \boldsymbol{\sigma}^{\mathrm{f}} + \boldsymbol{m}^{\mathrm{f}} = \mathbf{0}, \qquad \text{in } \mathcal{H}_t \sqcup \mathcal{B}_t. \tag{20}$$

If the fluid phase can be regarded as macroscopically inviscid and the constituents are assumed to be incompressible, the stress tensors of the solid and the fluid phase

can be chosen constitutively as [33, 34]

$$\boldsymbol{\sigma}^{\mathrm{s}} = -\varphi^{\mathrm{s}} p^{\mathrm{f}} \boldsymbol{I} + \boldsymbol{\sigma}^{\mathrm{s}}_{\mathrm{eff}}, \qquad \text{in } \mathcal{T}_t \sqcup \mathcal{H}_t \sqcup \mathcal{B}_t, \tag{21}$$

$$\boldsymbol{\sigma}^{\mathrm{f}} = -\varphi^{\mathrm{f}} p^{\mathrm{f}} \boldsymbol{I}, \qquad \text{in } \mathcal{T}_t \sqcup \mathcal{H}_t \sqcup \mathcal{B}_t, \tag{22}$$

in which $\boldsymbol{I}$ is the identity tensor, p^{f} represents the fluid pressure, and $\boldsymbol{\sigma}^{\mathrm{s}}_{\mathrm{eff}}$ is referred to as the *effective* Cauchy stress tensor of the solid phase.

To complete the mathematical model, we recall that the sets of equations (1)-(14) and (15)-(20) must be accompanied by the following interface conditions, which apply at the internal boundaries separating the three subdomains $\mathcal{T}_t$, $\mathcal{H}_t$, and $\mathcal{B}_t$:

$$\begin{cases} \boldsymbol{v}^{\mathrm{s}} \cdot \boldsymbol{n}\big|_{\mathcal{I}^{\alpha\beta}} = \boldsymbol{v}^{\mathrm{s}} \cdot \boldsymbol{n}\big|_{\mathcal{I}^{\beta\alpha}}, \\ \varphi^{\mathrm{f}} \rho^{\mathrm{f}} \boldsymbol{v}^{\mathrm{f}} \cdot \boldsymbol{n}\big|_{\mathcal{I}^{\alpha\beta}} = \varphi^{\mathrm{f}} \rho^{\mathrm{f}} \boldsymbol{v}^{\mathrm{f}} \cdot \boldsymbol{n}\big|_{\mathcal{I}^{\beta\alpha}}, \\ \left(\varphi^{\mathrm{f}} \rho^{\mathrm{f}} \omega^{\mathrm{N}} \boldsymbol{v}^{\mathrm{f}} + \boldsymbol{J}^{\mathrm{N}}\right) \cdot \boldsymbol{n}\big|_{\mathcal{I}^{\alpha\beta}} = \left(\varphi^{\mathrm{f}} \rho^{\mathrm{f}} \omega^{\mathrm{N}} \boldsymbol{v}^{\mathrm{f}} + \boldsymbol{J}^{\mathrm{N}}\right) \cdot \boldsymbol{n}\big|_{\mathcal{I}^{\beta\alpha}}, \\ \left(\boldsymbol{\sigma}^{\mathrm{s}} + \boldsymbol{\sigma}^{\mathrm{f}}\right) \cdot \boldsymbol{n}\big|_{\mathcal{I}^{\alpha\beta}} = \left(\boldsymbol{\sigma}^{\mathrm{s}} + \boldsymbol{\sigma}^{\mathrm{f}}\right) \cdot \boldsymbol{n}\big|_{\mathcal{I}^{\beta\alpha}}, \\ \omega^{\mathrm{N}}\big|_{\mathcal{I}^{\alpha\beta}} = \omega^{\mathrm{N}}\big|_{\mathcal{I}^{\beta\alpha}}, \\ p^{\mathrm{f}}\big|_{\mathcal{I}^{\alpha\beta}} = p^{\mathrm{f}}\big|_{\mathcal{I}^{\beta\alpha}}, \end{cases} \tag{23}$$

where $\mathcal{I}^{\alpha\beta}$ is the interface between the αth and the βth subdomain, with $\alpha, \beta = \mathcal{T}_t, \mathcal{H}_t, \mathcal{B}_t$, and $\boldsymbol{n}$ is the unit vector normal to $\mathcal{I}^{\alpha\beta}$. We emphasize that the conditions on $\boldsymbol{v}^{\mathrm{s}} \cdot \boldsymbol{n}$, ω^{N}, and p^{f} require these quantities to be continuous across the interface, whereas all other conditions are interface balance laws.

2.2 Stress tensor and mechanical response

To assess the mechanical response of the system considered in this work, it is crucial to remark that, similarly to K_t, also an undeformed (reference) configuration of the whole system, K_0, can be determined. The latter can be written as the disjoint union $K_0 = \mathcal{T}_0 \sqcup \mathcal{H}_0 \sqcup \mathcal{B}_0$. Here, $\mathcal{T}_0$, $\mathcal{H}_0$, and $\mathcal{B}_0$ denote, respectively, the subdomains occupied by the tumor tissue, the soft host tissue, and the bone, each in its undeformed (sub)configuration. By introducing the solid motion as the one-parameter of mappings

$$\chi^{\mathrm{s}}(\,\cdot\,,t) : K_0 \to \mathbf{R}^3, \quad X \mapsto x = \chi^{\mathrm{s}}(X,t) \in K_t \subset \mathbf{R}^3, \tag{24}$$

where $\mathbf{R}^3$ denotes here the three-dimensional Euclidean space, it is possible to map the global reference configuration K_0 into $K_t = \chi^{\mathrm{s}}(K_0,t)$. More specifically, the mappings $\chi^{\mathrm{s}}(\,\cdot\,,t)$ are continuous throughout K_0, which means that the subdomains $\mathcal{T}_0$, $\mathcal{H}_0$, and $\mathcal{B}_0$ are mapped into $\mathcal{T}_t = \chi^{\mathrm{s}}(\mathcal{T}_0,t)$, $\mathcal{H}_t = \chi^{\mathrm{s}}(\mathcal{H}_0,t)$, and $\mathcal{B}_t = \chi^{\mathrm{s}}(\mathcal{B}_0,t)$, respectively. Moreover, vectors attached to the points X of the subdomains $\mathcal{T}_0$, $\mathcal{H}_0$, and $\mathcal{B}_0$ are mapped into vectors attached to the points $x = \chi^{\mathrm{s}}(X,t)$ of $\mathcal{T}_t$, $\mathcal{H}_t$, and $\mathcal{B}_t$ through the deformation gradient tensor $\boldsymbol{F}$, whose components are expressed by $F_{iI} = \partial\chi^{\mathrm{s}}_i/\partial X_I$, $i,I = 1,2,3$, in appropriate coordinate systems. However, since $\chi^{\mathrm{s}}(\,\cdot\,,t)$ is generally not differentiable over all K_0 (see the interface condition (23)), but only piecewise differentiable (i.e., differentiable in each subdomain), the tensor $\boldsymbol{F}$ is piecewise continuous in K_0 and, consequently, it has to be defined separately for each subdomain.

Because of the growth and remodeling occurring in the system, which lead to variations of mass and shape as well as to a reorganization of its internal structure, the global undeformed configuration K_0 is generally not stress-free. To achieve a stress-free state (also referred to as *natural state* in the literature), K_t (or K_0) should be torn up in small stress-free pieces. However, since the particles constituting the subdomains of K_t have different material properties (indeed, neither K_t nor K_0 represent a uniform body), each of its subdomains must be brought to a natural state that is in general different from the other ones. To this end, we denote by $\mathcal{T}_\nu$, $\mathcal{H}_\nu$, and $\mathcal{B}_\nu$ the collections of stress-free body elements of $\mathcal{T}_t$, $\mathcal{H}_t$, and $\mathcal{B}_t$, respectively[1]. In particular, we notice that, since the bone is assumed to undergo neither growth nor remodeling, the collection $\mathcal{B}_\nu$ may be identified with the undeformed configuration $\mathcal{B}_0$.

A fundamental hypothesis of our model is that both the tumor and the soft host tissue exhibit hyperelastic behavior from the relaxed states $\mathcal{T}_\nu$ and $\mathcal{H}_\nu$, respectively. To account for this constitutive prescription in conjunction with growth and structural evolution, we invoke the theory of evolving natural "configurations" [25]. We use the quotation marks to emphasize that the relaxed states $\mathcal{T}_\nu$ and $\mathcal{H}_\nu$ are conglomerates of stress-free body pieces and, as such, they generally do not form a configuration in the proper sense of the word. We start with the description of the mechanical response of the tumor. As anticipated above, we consider the mechanical evolution of this tissue as dictated by three phenomena: growth, plastic reorganization, and elastic distortion. Hence, we introduce the multiplicative decomposition

[1]Note that, in general, these collections of relaxed body elements do not make a configuration.

of the deformation gradient tensor $\boldsymbol{F}$ [22, 23, 35, 24, 36], as:

$$\boldsymbol{F} = \boldsymbol{F}_{\mathrm{e}}\boldsymbol{F}_{\mathrm{a}} = \boldsymbol{F}_{\mathrm{e}}\boldsymbol{F}_{\mathrm{p}}\boldsymbol{F}_{\mathrm{g}}, \quad \text{in } \mathcal{T}_0. \tag{25}$$

In (25), $\boldsymbol{F}$ is related to the global change of shape of the body, $\boldsymbol{F}_{\mathrm{a}}$ represents the total anelastic distortions responsible for the evolution of the internal structure of the body, and $\boldsymbol{F}_{\mathrm{e}}$ describes the total elastic distortion. Note that $\boldsymbol{F}_{\mathrm{a}}$ maps vectors attached to $\mathcal{T}_0$ into vectors attached to $\mathcal{T}_\nu$, and $\boldsymbol{F}_{\mathrm{e}}$ map vectors of $\mathcal{T}_\nu$ into vectors of $\mathcal{T}_t$. To sketch the conceptual meaning of (25), we follow the explanation given in [37]. Hence, we consider a body that is brought from $\mathcal{T}_0$ to its current configuration $\mathcal{T}_t$ by the action of external loads. These, in general, are responsible for varying both the shape and the internal structure of the body in $\mathcal{T}_0$. If structural changes occur, it is not possible to bring back the body to $\mathcal{T}_0$ by simply removing the external loads. Rather, if all the external loads were switched off, the body would occupy a configuration, different from both $\mathcal{T}_t$ and $\mathcal{T}_0$, in which residual stresses may be present. To eliminate these, one should ideally tear the body into small disjoint pieces, and let each of them individually attain $\mathcal{T}_\nu$. Note that, as the body elements in $\mathcal{T}_\nu$ may turn out to be geometrically incompatible, $\mathcal{T}_\nu$ cannot be generally regarded as a configuration in Euclidean space. According to Figure 1, we can then split the map from $\mathcal{T}_0$ to $\mathcal{T}_\nu$ in two parts: the first, described by $\boldsymbol{F}_{\mathrm{g}}$, is related to growth and death processes, leading to possible changes in the mass of the volume element; the second, given by $\boldsymbol{F}_{\mathrm{p}}$, is due to internal reorganization of the body, in terms of rearranging of the adhesion bonds between the cells.

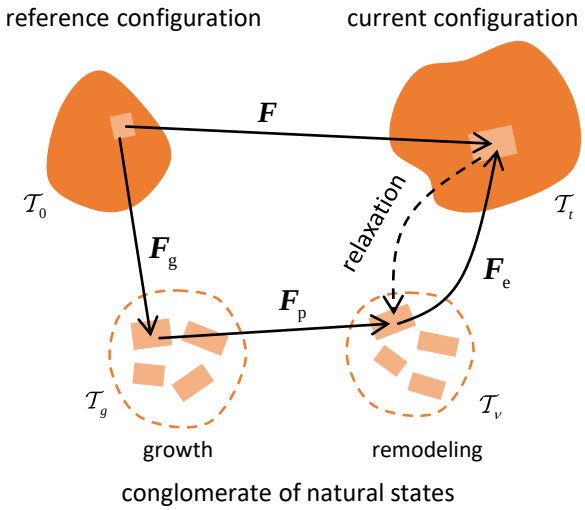

Figure 1: Schematic representation of the multiplicative decomposition of the deformation gradient tensor.

The determinant J of the deformation gradient $\boldsymbol{F}$ can be written as:

$$J = J_{\mathrm{e}} J_{\mathrm{a}} = J_{\mathrm{e}} J_{\mathrm{p}} J_{\mathrm{g}}, \tag{26}$$

where $J_{\mathrm{i}} = \det(\boldsymbol{F}_{\mathrm{i}})$ and $\mathrm{i} = \mathrm{e}, \mathrm{p}, \mathrm{g}$. We assume $\boldsymbol{F}_{\mathrm{g}}$ to be purely volumetric, i.e. $\boldsymbol{F}_{\mathrm{g}} = g\boldsymbol{I}$, and $\boldsymbol{F}_{\mathrm{p}}$ to be purely isochoric. It follows that $J_{\mathrm{g}} = g^3$, whereas $J_{\mathrm{p}} = 1$.

In the sequel, we assume that the soft host tissue experiences remodeling (i.e., a plastic reorganization of its internal structure). Thus, we specialize the decomposition (25) to the case of no growth by setting

$$\boldsymbol{F} = \boldsymbol{F}_{\mathrm{e}} \boldsymbol{F}_{\mathrm{a}} = \boldsymbol{F}_{\mathrm{e}} \boldsymbol{F}_{\mathrm{p}}, \qquad \text{in } \mathcal{H}_0, \tag{27}$$

with $\boldsymbol{F}_{\mathrm{a}} = \boldsymbol{F}_{\mathrm{p}}$. Again, the determinant of the deformation gradient will be given by:

$$J = J_{\mathrm{e}} J_{\mathrm{a}} = J_{\mathrm{e}} J_{\mathrm{p}}, \tag{28}$$

with $J_{\mathrm{a}} = J_{\mathrm{p}} = 1$. Note that the deformation gradient tensor is decomposed in the same manner both for the tumor and for the soft host tissue. However, in the latter we assume that no growth is present, leading to the identities $\boldsymbol{F}_{\mathrm{g}} = \boldsymbol{I}$ and $g = 1$.

The strain energy density of the system per unit volume of the undeformed configuration K_0 is denoted by

$$\mathcal{W}_0 = \begin{cases} J_{\mathrm{a}} \mathcal{W}_\nu^{\mathrm{t}} = J_{\mathrm{p}} J_{\mathrm{g}} \mathcal{W}_\nu^{\mathrm{t}}, & \text{in } \mathcal{T}_0, \\ J_{\mathrm{a}} \mathcal{W}_\nu^{\mathrm{h}} = J_{\mathrm{p}} \mathcal{W}_\nu^{\mathrm{h}}, & \text{in } \mathcal{H}_0, \\ \mathcal{W}_0^{\mathrm{b}}, & \text{in } \mathcal{B}_0, \end{cases} \tag{29}$$

where $\mathcal{W}_\nu^{\mathrm{t}}$ and $\mathcal{W}_\nu^{\mathrm{h}}$ are the energy densities per unit volume of the natural state of the tumor and of the soft host tissue, respectively, and $\mathcal{W}_0^{\mathrm{b}}$ is the energy density of the bone per unit volume of the undeformed configuration $\mathcal{B}_0$. We start with the description of the mechanical response of the tumor and of the soft host tissue. Since the materials are assumed to be isotropic, the strain energy densities can be written as a function of the first three invariants of the elastic right Cauchy-Green deformation tensor $\boldsymbol{C}_{\mathrm{e}} = \boldsymbol{F}_{\mathrm{e}}^T \boldsymbol{F}_{\mathrm{e}}$. In particular, we have

$$\mathcal{W}_\nu^{\mathrm{i}}(\boldsymbol{C}_{\mathrm{e}}) = \tilde{\mathcal{W}}_\nu^{\mathrm{i}}(I_1, I_2, I_3), \qquad \mathrm{i}{=}\mathrm{t,h}, \tag{30}$$

where

$$I_1 = \mathrm{tr}\left(\boldsymbol{C}_\mathrm{e}\right), \tag{31}$$

$$I_2 = \frac{1}{2}\left[I_1^2 - \mathrm{tr}\left(\boldsymbol{C}_\mathrm{e}^2\right)\right], \tag{32}$$

$$I_3 = \det\left(\boldsymbol{C}_\mathrm{e}\right), \tag{33}$$

and $\boldsymbol{C}_\mathrm{e}$ is expressed piecewise as

$$\boldsymbol{C}_\mathrm{e} = \boldsymbol{F}_\mathrm{a}^{-T}\boldsymbol{C}\boldsymbol{F}_\mathrm{a}^{-1} = \begin{cases} g^{-2}\boldsymbol{F}_\mathrm{p}^{-T}\boldsymbol{C}\boldsymbol{F}_\mathrm{p}^{-1}, & \text{in } \mathcal{T}_0, \\ \boldsymbol{F}_\mathrm{p}^{-T}\boldsymbol{C}\boldsymbol{F}_\mathrm{p}^{-1}, & \text{in } \mathcal{H}_0, \end{cases} \tag{34}$$

$$\mathrm{tr}\left(\boldsymbol{C}_e\right) = \mathrm{tr}\left(\boldsymbol{C}\boldsymbol{B}_\mathrm{a}\right) = \begin{cases} g^{-2}\mathrm{tr}\left(\boldsymbol{C}\boldsymbol{B}_\mathrm{p}\right), & \text{in } \mathcal{T}_0, \\ \mathrm{tr}\left(\boldsymbol{C}\boldsymbol{B}_\mathrm{p}\right), & \text{in } \mathcal{H}_0, \end{cases} \tag{35}$$

$$\boldsymbol{B}_\mathrm{a} = \boldsymbol{F}_\mathrm{a}^{-1}\boldsymbol{F}_\mathrm{a}^{-T} = \begin{cases} g^{-2}\boldsymbol{B}_\mathrm{p}, & \text{in } \mathcal{T}_0, \\ \boldsymbol{B}_\mathrm{p}, & \text{in } \mathcal{H}_0. \end{cases} \tag{36}$$

From the expression of the energy we can calculate the solid phase second Piola-Kirchhoff stress tensor associated with the natural state of the subdomains $\mathcal{T}_0$ and $\mathcal{H}_0$:

$$\begin{aligned} \boldsymbol{S}^\mathrm{i}_{\nu,\mathrm{eff}} &= 2\frac{\partial \mathcal{W}^\mathrm{i}_\nu}{\partial \boldsymbol{C}_\mathrm{e}} = \sum_{j=1}^{3} 2\frac{\partial \mathcal{W}^\mathrm{i}_\nu}{\partial I_j}\frac{\partial I_j}{\partial \boldsymbol{C}_\mathrm{e}} = \sum_{j=1}^{3} 2b^\mathrm{i}_j \frac{\partial I_j}{\partial \boldsymbol{C}_\mathrm{e}} \\ &= \left(2b^\mathrm{i}_1 + 2b^\mathrm{i}_2 I_1\right)\boldsymbol{I} - 2b^\mathrm{i}_2\boldsymbol{C}_\mathrm{e} + 2b^\mathrm{i}_3 I_3 \boldsymbol{C}_\mathrm{e}^{-1}. \end{aligned} \tag{37}$$

with $b^{\mathrm{i}}_j = \frac{\partial \mathcal{W}^{\mathrm{i}}_\nu}{\partial I_j}$, and $\mathrm{i} = \mathrm{t}, \mathrm{h}$. Note that the second Piola-Kirchhoff stress tensor associated with the reference configuration can be obtained as the Piola transformation $\boldsymbol{S}^{\mathrm{i}}_{\mathrm{eff}} = J_{\mathrm{a}} \boldsymbol{F}^{-1}_{\mathrm{a}} \boldsymbol{S}^{\mathrm{i}}_{\nu,\mathrm{eff}} \boldsymbol{F}^{-T}_{\mathrm{a}}$.

When the material response of the tumor is considered, for $\mathrm{i} = \mathrm{t}$, the effective second Piola-Kirchhoff stress tensor is a constitutive function of $\boldsymbol{F}$, g, and $\boldsymbol{B}_{\mathrm{p}}$, i.e., $\boldsymbol{S}^{\mathrm{t}}_{\mathrm{eff}} = \boldsymbol{S}^{\mathrm{t}}_{\mathrm{eff}}\left(\boldsymbol{F}, g, \boldsymbol{B}_{\mathrm{p}}\right)$. Moreover, recalling that the plastic distortions are isochoric, i.e., $J_{\mathrm{p}} = 1$, we finally obtain

$$\boldsymbol{S}^{\mathrm{t}}_{\mathrm{eff}} = 2g b^{\mathrm{t}}_1 \boldsymbol{B}_{\mathrm{p}} + 2b^{\mathrm{t}}_2 \frac{1}{g}\left[\mathrm{tr}\left(\boldsymbol{C}\boldsymbol{B}_{\mathrm{p}}\right)\boldsymbol{B}_{\mathrm{p}} - \boldsymbol{B}_{\mathrm{p}}\boldsymbol{C}\boldsymbol{B}_{\mathrm{p}}\right] + 2b^{\mathrm{t}}_3 \frac{J^2}{g^3}\boldsymbol{C}^{-1}. \tag{38}$$

It is worth to remark that, by virtue of the hypothesis of isotropy, the plastic behavior of the system can be formulated in terms of $\boldsymbol{B}_{\mathrm{p}}$, rather than $\boldsymbol{F}_{\mathrm{p}}$. Although, on the one hand, this leads to a loss of information, on the other hand, it brings about important simplifications. In this work, we assume the Holmes and Mow form [38] for the strain energy densities of the tumor and of the soft host tissue. This constitutive behavior is able to capture the mechanical characteristics of soft hydrated tissues and is expressed by the formula:

$$\mathcal{W}^{\mathrm{i}}_\nu = a^{\mathrm{i}}_0\left[\exp\left(\Psi\right) - 1\right], \;\; \Psi = a^{\mathrm{i}}_1\left(I_1 - 3\right) + a^{\mathrm{i}}_2\left(I_2 - 3\right) - \beta^{\mathrm{i}}\ln\left(I_3\right), \tag{39}$$

where i=t,h, and a^{i}_0, a^{i}_1, a^{i}_2, β^{i} are coefficients related to material properties, i.e.,

$$a^{\mathrm{i}}_0 = \frac{2\mu^{\mathrm{i}} + \lambda^{\mathrm{i}}}{4}, \quad a^{\mathrm{i}}_1 = \frac{2\mu^{\mathrm{i}} - \lambda^{\mathrm{i}}}{2\mu^{\mathrm{i}} + \lambda^{\mathrm{i}}}, \quad a^{\mathrm{i}}_2 = \frac{\lambda^{\mathrm{i}}}{2\mu^{\mathrm{i}} + \lambda^{\mathrm{i}}}, \quad \beta^{\mathrm{i}} = a^{\mathrm{i}}_1 + 2a^{\mathrm{i}}_2, \tag{40}$$

Here, λ^{i} and μ^{i} are the Lamé constants of the solid scaffold, and β^{i} is usually assumed to be one. In equation (38), b^{i}_j, $j = 1, 2, 3$, can be calculated from (37) as

$$b^{\mathrm{i}}_1 = a^{\mathrm{i}}_1 \left(\mathcal{W}^{\mathrm{i}}_\nu + a^{\mathrm{i}}_0\right), \tag{41}$$

$$b^{\mathrm{i}}_2 = a^{\mathrm{i}}_2 \left(\mathcal{W}^{\mathrm{i}}_\nu + a^{\mathrm{i}}_0\right), \tag{42}$$

$$b^{\mathrm{i}}_3 = -\frac{\beta^{\mathrm{i}}}{I_3} \left(\mathcal{W}^{\mathrm{i}}_\nu + a^{\mathrm{i}}_0\right). \tag{43}$$

The relations in (41)-(43) can be substituted into the expression (38) for the solid stress in the reference configuration.

Concerning the effective stress of the bone tissue, we choose an energy density function of the Saint Venant-Kirchhoff type as

$$\mathcal{W}^{\mathrm{b}}_0(\boldsymbol{E}) = \mu^{\mathrm{b}} \operatorname{tr}(\boldsymbol{E}^2) + \frac{\lambda^{\mathrm{b}}}{2}[\operatorname{tr}(\boldsymbol{E})]^2, \tag{44}$$

where μ^{b} and λ^{b} are the shear modulus and the first Lamé parameter of the bone, respectively, and $\boldsymbol{E} = \frac{1}{2}(\boldsymbol{C} - \boldsymbol{I})$ is the Green-Lagrange strain tensor. Consequently, the constitutive part of the stress associated to the bone is given by

$$\boldsymbol{S}^{\mathrm{b}}_{\mathrm{eff}} = 2\mu^{\mathrm{b}}\, \boldsymbol{E} + \lambda^{\mathrm{b}} \operatorname{tr}(\boldsymbol{E})\boldsymbol{I}. \tag{45}$$

The momentum equation (14) of the whole biphasic system rephrases, in the material configuration, as

$$\operatorname{Div}\left(\boldsymbol{P}^{\mathrm{s}}_{\mathrm{eff}} - J p^{\mathrm{f}} \boldsymbol{F}^{-T}\right) = 0, \tag{46}$$

where Div$(\cdot)$ denotes the material divergence operator, and $\boldsymbol{P}^{\mathrm{s}}_{\mathrm{eff}} = \boldsymbol{F}\boldsymbol{S}^{\mathrm{s}}_{\mathrm{eff}}$. Since the system is subdivided into different tissue compartments, the stress can be evaluated as

$$\boldsymbol{S}^{\mathrm{s}}_{\mathrm{eff}} = \begin{cases} \boldsymbol{S}^{\mathrm{t}}_{\mathrm{eff}}, & \text{in } \mathcal{T}_0, \\ \boldsymbol{S}^{\mathrm{h}}_{\mathrm{eff}}, & \text{in } \mathcal{H}_0, \\ \boldsymbol{S}^{\mathrm{b}}_{\mathrm{eff}}, & \text{in } \mathcal{B}_0. \end{cases} \tag{47}$$

where the three $\boldsymbol{S}^{\mathrm{i}}_{\mathrm{eff}}$ have been defined in (38) and (45), respectively.

The last equation in the model is the one governing the plastic distortions. This can be expressed in terms of the time derivative of $\boldsymbol{B}_{\mathrm{p}}$ as [28, 30, 32, 37, 39]:

$$\dot{\boldsymbol{B}}_{\mathrm{p}} = -\frac{2\lambda_{\mathrm{p}}}{\|\mathrm{dev}\,(\boldsymbol{\sigma}^{\mathrm{s}}_{\mathrm{eff}})\|}\left\langle \|\mathrm{dev}\,(\boldsymbol{\sigma}^{\mathrm{s}}_{\mathrm{eff}})\| - \sqrt{2/3}\sigma_{\mathrm{y}} \right\rangle_{+} \boldsymbol{B}_{\mathrm{p}}\,\mathrm{dev}\,(\boldsymbol{\Sigma}^{\mathrm{s}}_{\mathrm{eff}})\,, \tag{48}$$

where we denote by dev$(\cdot)$ the deviatoric part of the tensor to which it is applied $(\mathrm{i} = \mathrm{t}, \mathrm{h})$. Note that the use of $\boldsymbol{B}_{\mathrm{p}}$, rather than $\boldsymbol{F}_{\mathrm{p}}$, as a measure of plastic deformations is allowed by the hypothesis of material isotropy [40, 41, 37]. In (48), $\boldsymbol{\sigma}^{\mathrm{s}}_{\mathrm{eff}}$ is the effective Cauchy stress in the solid phase, obtained from the second Piola-Kirchhoff tensor by the Piola transformation:

$$\boldsymbol{\sigma}^{\mathrm{s}}_{\mathrm{eff}} = \frac{1}{J}\boldsymbol{F}\boldsymbol{S}^{\mathrm{s}}_{\mathrm{eff}}\boldsymbol{F}^{T}. \tag{49}$$

Then, σ_{y} is the yield stress, above which the plastic flow starts (as indicated by the Macaulay brackets $\langle\cdot\rangle_{+}$ such that $\langle f\rangle_{+} = f$ if $f > 0$ and $\langle f\rangle_{+} = 0$ otherwise).

Finally, $\boldsymbol{\Sigma}^{\mathrm{s}}_{\mathrm{eff}}$ is the material Mandel stress tensor in the solid phase, given by $\boldsymbol{\Sigma}^{\mathrm{s}}_{\mathrm{eff}} = \boldsymbol{F}^T \boldsymbol{P}^{\mathrm{s}}_{\mathrm{eff}}$. This remodeling activates in the tumor and in the soft host tissue, with a different value of the yield stress for each tissue ($\sigma^{\mathrm{t}}_{\mathrm{y}}$ and $\sigma^{\mathrm{h}}_{\mathrm{y}}$, respectively).

Notice that the equation for the plastic flow constitutes a phenomenological description of phenomena occurring at the cell scale: If we consider a cluster of cells subjected to a sufficiently high tension, some of their adhesive bonds may break and reform in other places. The mechanical energy required by the system for breaking the bonds and reforming them in other places is not stored, being dissipated during the process. Moreover, a cell aggregate subjected to a given load after reorganization will respond elastically for small loads, as long as the bonds are not broken again [28]. The law in (48) is thus stating the following: if the stress in the material is below a given threshold, denoted here by σ_{y}, then the derivative of $\boldsymbol{B}_{\mathrm{p}}$ is zero and no plastic flow occurs. When the stress exceeds the threshold, the material evolves to release the stress in excess, until the yield stress is reached or exceeded again. The parameter λ_{p} gives an indication of the characteristic time for cell reorganization and the following stress relaxation.

2.3 Constitutive relations for the mass exchange terms

The exchange term Γ^{s} appearing in equation (4) is related to tumor cell proliferation and death. Recalling equation (7), it is given by the sum of $\Gamma^{\mathrm{p}}_{\mathrm{f}\to\mathrm{p}}$ and $\Gamma^{\mathrm{n}}_{\mathrm{n}\to\mathrm{f}}$. The first quantity describes tumor growth and reads

$$\Gamma^{\mathrm{p}}_{\mathrm{f}\to\mathrm{p}} = \gamma^{\mathrm{p}}_{\mathrm{fp}} \left\langle \frac{\omega^{\mathrm{N}} - \omega^{\mathrm{N}}_{\mathrm{cr}}}{\omega^{\mathrm{N}}_{\mathrm{env}} - \omega^{\mathrm{N}}_{\mathrm{cr}}} \right\rangle_{+} \left(1 - \frac{\delta_1 \langle \bar{\sigma}^{\mathrm{s}}_{\mathrm{eff}} \rangle_{+}}{\langle \bar{\sigma}^{\mathrm{s}}_{\mathrm{eff}} \rangle_{+} + \delta_2} \right) \frac{\varphi^{\mathrm{f}}}{\varphi^{\mathrm{f}}_0} \omega^{\mathrm{p}} \varphi^{\mathrm{s}}, \tag{50}$$

where the coefficient $\gamma^{\mathrm{p}}_{\mathrm{fp}} \geq 0$ accounts for the nutrient uptake and for the mass of the interstitial fluid that becomes tumor due to cell growth, $\omega^{\mathrm{N}}_{\mathrm{cr}}$ is the critical level of oxygen below which cell proliferation is inhibited, $\omega^{\mathrm{N}}_{\mathrm{env}}$ is the mass fraction of oxygen in the environment, $\bar{\sigma}^{\mathrm{s}}_{\mathrm{eff}}$ is the spherical part of the effective Cauchy stress tensor associated with the solid phase, i.e., $\bar{\sigma}^{\mathrm{s}}_{\mathrm{eff}} = -\mathrm{tr}(\boldsymbol{\sigma}^{\mathrm{s}}_{\mathrm{eff}})/3$, and the positive constants δ_1 and δ_2 (with $\delta_1 < 1$) account for the action of mechanical stress on cell proliferation. Due to its form, the term in parentheses in (50) describes growth inhibition due to tumor compression. Finally, φ^{f}_0 is the initial volume fraction of the fluid phase. The second part of Γ^{s}, namely $\Gamma^{\mathrm{n}}_{\mathrm{n}\to\mathrm{f}}$, takes the form:

$$\Gamma^{\mathrm{n}}_{\mathrm{n}\to\mathrm{f}} = -\gamma^{\mathrm{n}}_{\mathrm{nf}}\omega^{\mathrm{n}}\varphi^{\mathrm{s}}. \tag{51}$$

This term is related to cell death from lysis in the necrotic population of the tumor. The coefficient $\gamma^{\mathrm{n}}_{\mathrm{nf}}$ takes into account the degradation of cellular membranes and the mass conversion into interstitial fluid. Then, the rate of tumor cell death in equation (2) is described by the relation

$$\Gamma^{\mathrm{p}}_{\mathrm{p}\to\mathrm{n}} = -\gamma^{\mathrm{p}}_{\mathrm{pno}}\left\langle 1 - \frac{\omega^{\mathrm{N}}}{\omega^{\mathrm{N}}_{\mathrm{cr}}}\right\rangle_{+}\omega^{\mathrm{p}}\varphi^{\mathrm{s}}, \tag{52}$$

where the parameter $\gamma^{\mathrm{p}}_{\mathrm{pno}}$ is related to the rate of cell necrosis. In this way, we assume cell death to occur solely by nutrient deprivation. Finally, nutrient consumption by tumor cells is described by:

$$\Gamma^{\mathrm{N}}_{\mathrm{N}\to\mathrm{p}} = -\gamma^{\mathrm{N}}_{\mathrm{Np1}}\frac{\omega^{\mathrm{N}}}{\omega^{\mathrm{N}} + \gamma^{\mathrm{N}}_{\mathrm{Np2}}}\omega^{\mathrm{p}}\varphi^{\mathrm{s}}. \tag{53}$$

Here, $\gamma^{\mathrm{N}}_{\mathrm{Np1}}$ and $\gamma^{\mathrm{N}}_{\mathrm{Np2}}$ are two coefficients regulating nutrient uptake by the cells. Note that the mathematical expressions adopted for the mass exchange terms are similar to the ones reported in [42], validated with data from tumor spheroid experiments.

3 Benchmark Tests

3.1 Summary of the model equations

In this Section, we summarize the final form of the equations of the model. A thorough derivation is available in Appendix A. Granted that φ^{s} can be expressed as

$$\varphi^{\mathrm{s}} = \frac{g^3 \varphi^{\mathrm{s}}_{\nu}}{J}, \tag{54}$$

where $\varphi^{\mathrm{s}}_{\nu}$ is the solid volume fraction in the natural state, the final system of equations to be solved is given by

$$\frac{\dot{g}}{g} = \frac{1}{3}\frac{\Gamma^{\mathrm{s}}}{\varphi^{\mathrm{s}}\rho}, \tag{55}$$

$$\dot{\omega}^{\mathrm{p}} = \frac{J}{\rho \varphi^{\mathrm{s}}_{\nu} g^3}\left(\Gamma^{\mathrm{p}}_{\mathrm{p}\to\mathrm{n}} + \Gamma^{\mathrm{p}}_{\mathrm{f}\to\mathrm{p}} - \omega^{\mathrm{p}}\Gamma^{\mathrm{s}}\right), \tag{56}$$

$$J\varphi^{\mathrm{f}}\rho\dot{\omega}^{\mathrm{N}} + \rho \boldsymbol{Q}\cdot \operatorname{Grad}\omega^{\mathrm{N}} + \operatorname{Div}\left(\boldsymbol{\Psi}^{\mathrm{N}}\right) = J\left(\Gamma^{\mathrm{N}}_{\mathrm{N}\to\mathrm{p}} + \omega^{\mathrm{N}}\Gamma^{\mathrm{s}}\right), \tag{57}$$

$$\operatorname{Div}\left(\boldsymbol{Q}\right) + \dot{J} = 0, \tag{58}$$

$$\operatorname{Div}\left(\boldsymbol{P}^{\mathrm{s}}_{\mathrm{eff}} - Jp^{\mathrm{f}}\boldsymbol{F}^{-T}\right) = 0, \tag{59}$$

$$\dot{\boldsymbol{B}}_p = -\frac{2\lambda_{\mathrm{p}}}{\|\operatorname{dev}\left(\boldsymbol{\sigma}^{\mathrm{s}}_{\mathrm{eff}}\right)\|}\left\langle \|\operatorname{dev}\left(\boldsymbol{\sigma}^{\mathrm{s}}_{\mathrm{eff}}\right)\| - \sqrt{2/3}\sigma_{\mathrm{y}}\right\rangle_{+}\boldsymbol{B}_{\mathrm{p}}\operatorname{dev}\left(\boldsymbol{\Sigma}^{\mathrm{s}}_{\mathrm{eff}}\right), \tag{60}$$

where we introduced the Piola transformations of Darcy's filtration velocity and Fick's mass flux

$$\boldsymbol{Q} = J\boldsymbol{F}^{-1}\varphi^{\mathrm{f}}\left(\boldsymbol{v}^{\mathrm{f}} - \boldsymbol{v}^{\mathrm{s}}\right) = -J\boldsymbol{F}^{-1}\boldsymbol{k}\boldsymbol{F}^{-T}\mathrm{Grad}\, p^{\mathrm{f}}, \tag{61}$$

$$\boldsymbol{\Psi}^{\mathrm{N}} = -J\varphi^{\mathrm{f}}\rho\boldsymbol{F}^{-1}\boldsymbol{D}^{\mathrm{N}}\boldsymbol{F}^{-T}\mathrm{Grad}\,\omega^{\mathrm{N}}. \tag{62}$$

The system in (55)-(60) is to be solved for the free unknowns

$$\mathcal{U} = \{g, \omega^{\mathrm{p}}, \omega^{\mathrm{N}}, p^{\mathrm{f}}, \chi^{\mathrm{s}}, \boldsymbol{B}_{\mathrm{p}}\}. \tag{63}$$

Note that the system is closed, since it features 13 scalar unknowns and (55)-(60) constitute a set of 13 scalar equations. In (61) and (62), $\boldsymbol{k}$ and $\boldsymbol{D}^{\mathrm{N}}$ are two isotropic tensors describing nutrient diffusivity and tissue hydraulic conductivity. They are given by the expressions $\boldsymbol{k} = k\boldsymbol{I}$ and $\boldsymbol{D}^{\mathrm{N}} = D^{\mathrm{N}}\boldsymbol{I}$, respectively. The equations (55)-(62) are obtained under the hypotheses that the mass densities of the fluid and solid phases are constant and equal ($\rho^{\mathrm{s}} = \rho^{\mathrm{f}} = \rho$). In the following, we consider only one nutrient species, namely oxygen.

3.2 Description of the benchmarks

Hereafter, three benchmark tests are discussed. In the first case, we consider a tumor spheroid growing in the culture medium. In the second benchmark, the spheroid grows in a soft host tissue having spherical structure. Finally, in a third benchmark, we present the results of a tumor growing in a three-dimensional heterogeneous domain, in which the host tissue comprises both a soft material and a stiffer one,

identified with a bone tissue.

In the first case, the model consists of a sphere segment in axisymmetric conditions. The spheroid has an initial radius of 100 μm and the initial solid volume fraction φ^{s} is fixed at 0.8 over the domain. We assume the following initial conditions:

$$g = 1, \quad \omega^{\mathrm{p}} = 1, \quad \omega^{\mathrm{N}} = \omega^{\mathrm{N}}_{\mathrm{env}}, \quad p^{\mathrm{f}} = 0, \quad \boldsymbol{B}_{\mathrm{p}} = \boldsymbol{I}, \quad \text{in } \mathcal{T}_0. \tag{64}$$

Moreover, the boundary conditions for the problem are summarized in Figure 2.

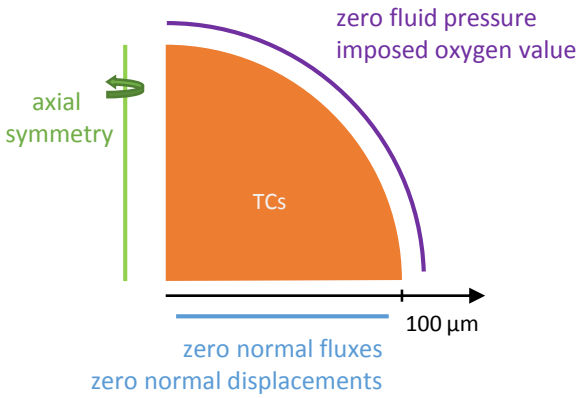

Figure 2: Geometry of the problem and boundary conditions for a tumor spheroid.

On the outer boundary of the spheroid, we assume a fixed value ($\omega^{\mathrm{N}}_{\mathrm{env}}$) for the nutrient mass fraction and zero interstitial fluid pressure. Due to the symmetry, no-flux boundary conditions are imposed normal to the radius of the sphere segment.

The parameters used for this first benchmark test come from different sources, and are reported in Table 1.

Regarding the values used for the plastic flow rule, we have referred to the work of Iordan *et al.* [51] for an estimate of the yield stress in the tumor tissue. In

Table 1: Parameters used in the model for the tumor spheroid.

Symbol	Parameter	Unit	Value	Reference
φ_ν^{s}	Solid volume fraction in the natural state	$(-)$	8.0×10^{-1}	[30]
ρ	Density of the phases	$\mathrm{kg/m^3}$	1.0×10^{3}	[43]
k	Tumor hydraulic conductivity	$\mathrm{m^2/(Pa \cdot s)}$	4.875×10^{-13}	[44]
D^{N}	Nutrient diffusion coefficient	$\mathrm{m^2/s}$	3.2×10^{-9}	[43]
$\omega_{\mathrm{cr}}^{\mathrm{N}}$	Critical level of nutrient	$(-)$	2.0×10^{-6}	[42]
$\omega_{\mathrm{env}}^{\mathrm{N}}$	Environmental level of nutrient	$(-)$	7.0×10^{-6}	[45, 46]
$\gamma_{\mathrm{Np1}}^{\mathrm{N}}$	Coefficient related to nutrient consumption	$\mathrm{kg/(m^3 \cdot s)}$	3.0×10^{-4}	[47, 48]
$\gamma_{\mathrm{Np2}}^{\mathrm{N}}$	Coefficient related to nutrient consumption	$(-)$	1.48×10^{-7}	[47, 48]
$\gamma_{\mathrm{fp}}^{\mathrm{p}}$	Coefficient related to growth	$\mathrm{kg/(m^3 \cdot s)}$	5.348×10^{-3}	[49]
$\gamma_{\mathrm{pno}}^{\mathrm{p}}$	Coefficient related to necrosis	$\mathrm{kg/(m^3 \cdot s)}$	1.5×10^{-1}	[42]
$\gamma_{\mathrm{nf}}^{\mathrm{n}}$	Coefficient related to lysis	$\mathrm{kg/(m^3 \cdot s)}$	1.15×10^{-2}	[42]
λ_{p}	Coefficient related to cell reorganization time	$\mathrm{1/(Pa \cdot s)}$	8.334×10^{-7}	[50]
$\sigma_{\mathrm{y}}^{\mathrm{t}}$	Yield stress	Pa	1.0×10^{1}	[51]
λ^{t}	Lamé's first parameter for the tumor	Pa	1.333×10^{4}	[44]
μ^{t}	Shear modulus for the tumor	Pa	1.999×10^{4}	[44]
δ_1	Coefficient related to growth inhibition	$(-)$	7.138×10^{-1}	[42]
δ_2	Coefficient related to growth inhibition	Pa	1.541×10^{3}	[42]

addition, the value for the coefficient λ_{p} is derived from the cell reorganization time τ_{p} by the expression:

$$\tau_{\mathrm{p}} \simeq \frac{1}{\mu^{\mathrm{t}} \lambda_{\mathrm{p}}},$$

where we have considered a value for τ_{p} of the order of one minute, consistently with the observations of Forgacs and colleagues [50]. The equations in the model were solved using the finite element software COMSOL Multiphysics® (COMSOL AB, Sweden).

In the second case, we consider the growth of an avascular tumor within a healthy tissue. As mentioned in the previous section, the soft host tissue is modeled as an elasto-visco-plastic solid where the elastic strain energy and the plastic flow rule are characterized by the same constitutive relations of the tumor. However, an

independent set of parameters is used for the healthy tissue, providing a different mechanical response. At the interfaces between the different domains, COMSOL applies automatically the conditions in (23). The geometry and boundary conditions of the problem are shown in Figure 3.

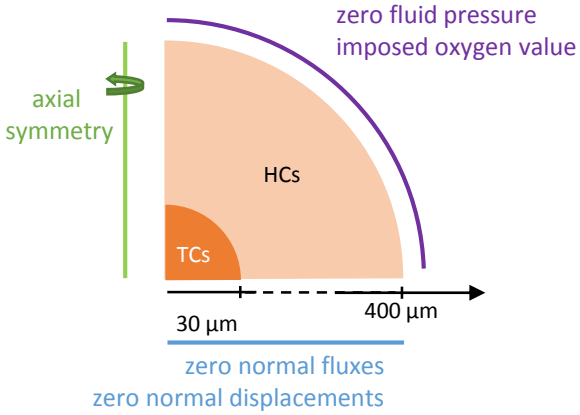

Figure 3: Geometry of the problem and boundary conditions for a tumor growing in a soft host tissue.

Similar to the numerical experiments in [43], the tumor and the host tissue are modeled as a sphere segment imposing cylindrical symmetry. The tumor occupies the region that is closer to the sphere center, with an initial radius of 30 μm. From there, the host tissue extends until the outer boundary of the computational domain, with an external radius of 400 μm. We consider an initial solid volume fraction equal to 0.7 throughout the domain. The initial conditions for the problem read:

$$g = 1, \quad \omega^{\mathrm{p}} = 1, \quad \text{in } \mathcal{T}_0, \tag{65}$$

$$\omega^{\mathrm{N}} = \omega^{\mathrm{N}}_{\mathrm{env}}, \quad p^{\mathrm{f}} = 0, \quad \boldsymbol{B}_{\mathrm{p}} = \boldsymbol{I} \quad \text{in } \mathcal{T}_0 \sqcup \mathcal{H}_0. \tag{66}$$

Regarding the boundary conditions, the nutrient mass fraction and the interstitial fluid pressure on the outer boundary are set equal to $\omega^{\mathrm{N}}_{\mathrm{env}}$ and zero, respectively. To take into account the presence of a host tissue, we select a value for $\omega^{\mathrm{N}}_{\mathrm{env}}$ that corresponds to the average dissolved oxygen in the plasma of a healthy individual [43]. Moreover, in this second case the growth coefficient $\gamma^{\mathrm{p}}_{\mathrm{fp}}$ and the critical value of oxygen $\omega^{\mathrm{N}}_{\mathrm{cr}}$ take different values from before. On the other boundaries, zero flux is imposed for the nutrient and the fluid due to the presence of the symmetry boundary. The parameters pertaining to the healthy tissue are given in Table 2, whereas all the other parameters are the same as in Table 1.

Table 2: Parameters used for the case of a tumor growing in a soft host tissue.

Symbol	Parameter	Unit	Value	Reference
λ^{h}	Lamé's first parameter for the soft host tissue	Pa	3.336×10^{3}	[52]
μ^{h}	Shear modulus for the soft host tissue	Pa	5.0×10^{3}	[52]
$\sigma^{\mathrm{h}}_{\mathrm{y}}$	Yield stress for the soft host tissue[a]	Pa	1.0×10^{3}	-
λ_{p}	Coefficient related to cell reorganization time	$1/(\mathrm{Pa} \cdot \mathrm{s})$	8.334×10^{-8}	-
$\gamma^{\mathrm{p}}_{\mathrm{fp}}$	Coefficient related to growth	$\mathrm{kg}/(\mathrm{m}^3 \cdot \mathrm{s})$	8.022×10^{-3}	[53]
$\omega^{\mathrm{N}}_{\mathrm{cr}}$	Critical level of nutrient	$(-)$	1.0×10^{-6}	-
$\omega^{\mathrm{N}}_{\mathrm{env}}$	Environmental level of nutrient	$(-)$	4.2×10^{-6}	[43]

[a] Value assumed when plastic rearrangement in the soft host tissue is taken into account.

We assume that cellular bonds are more stable for a tumor grown in a host tissue than as a spheroid, and impose a larger time for cell rearrangement and a higher value for the healthy tissue yield stress.

As a last case, we analyze the growth of a tumor in proximity to a blood capillary and two different host tissues. The blood vessel constitutes the only source of nutrient that influences the development of the spatial pattern of the tumor. A tissue with the mechanical properties of a bone occupies a portion of the domain, whereas a soft host tissue fills the rest of the geometry. We consider the ideal

geometry of Figure 4.a, where the capillary lies next to a spherical tumor.

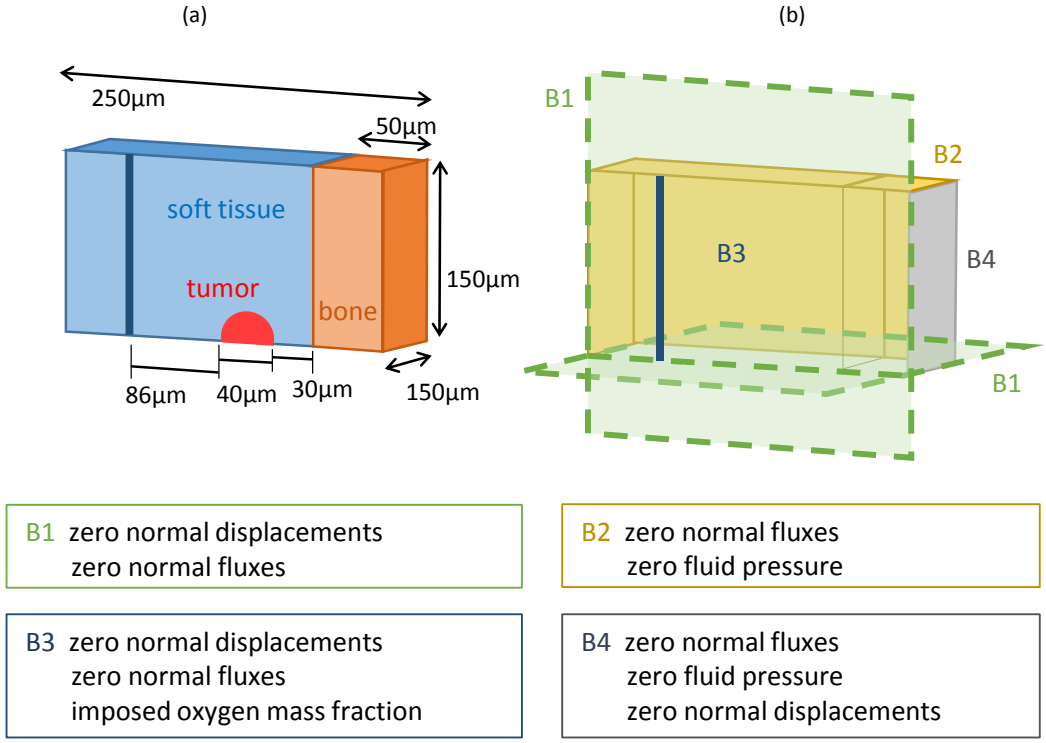

Figure 4: Geometry of the problem and boundary conditions for a tumor growing in a heterogeneous environment.

The capillary has a diameter of 8 μm and the tumor starts with an initial diameter of 40 μm. This geometry has two planes of symmetry, allowing to discretize only one quarter of the actual domain. Figure 4.a shows the size of the other compartments of the problem. We enable plastic deformations to develop in the soft host tissue, as well as in the tumor, and fix the value of the yield stress of the soft host tissue as $\sigma_{\mathrm{y}}^{\mathrm{h}} = 10^3$ Pa. We assume a higher value for the cell reorganization time than in the previous case, leading to a lower value for λ_{p}. The initial conditions of

the problem are stated below:

$$g = 1, \quad \omega^{\mathrm{p}} = 1, \quad \text{in } \mathcal{T}_0, \tag{67}$$

$$\boldsymbol{B}_{\mathrm{p}} = \boldsymbol{I}, \quad \text{in } \mathcal{T}_0 \sqcup \mathcal{H}_0, \tag{68}$$

$$\omega^{\mathrm{N}} = \omega^{\mathrm{N}}_{\mathrm{cap}}, \quad p^{\mathrm{f}} = 0, \quad \text{in } K_t. \tag{69}$$

Here $\omega^{\mathrm{N}}_{\mathrm{cap}}$ is the mass fraction of the nutrient supplied by the capillary. The boundary conditions for the problem are reported in Figure 4.b. In particular, the oxygen mass fraction is fixed on the cylindrical surfaces of the capillary, where we set it equal to $\omega^{\mathrm{N}}_{\mathrm{cap}}$. On the remaining lateral surfaces we impose zero oxygen flux. Because of symmetry properties of the problem, our simulations consider only one quarter of the overall geometry, and we need to impose symmetry boundary conditions for the pressure and for the displacements on the surface $B1 \cap K_0$ of Fig. 4.

The additional parameters for this case, including the mechanical response of the bone tissue, are summarized in Table 3.

Table 3: Additional parameters for the three-dimensional tumor model.

Symbol	Parameter	Unit	Value	Reference
λ^{b}	Lamé's first parameter for the bone tissue	Pa	5.769×10^{9}	[54, 55]
μ^{b}	Shear modulus for the bone tissue	Pa	3.846×10^{9}	[54, 55]
φ^{b}	Bone porosity	$(-)$	6.0×10^{-1}	[54, 55]
k^{b}	Bone hydraulic conductivity	$\mathrm{m}^2/(\mathrm{Pa} \cdot \mathrm{s})$	3.0×10^{-15}	[54, 55]
R_0	Tumor initial diameter	μm	40	-
$\omega^{\mathrm{N}}_{\mathrm{cap}}$	Capillary oxygen mass fraction	$(-)$	4.2×10^{-6}	[43]
$\omega^{\mathrm{N}}_{\mathrm{cr}}$	Critical oxygen mass fraction	$(-)$	3.0×10^{-6}	-
$\gamma^{\mathrm{p}}_{\mathrm{fp}}$	Coefficient related to growth	$\mathrm{kg}/(\mathrm{m}^3 \cdot \mathrm{s})$	1.0×10^{-2}	-
λ_{p}	Coefficient related to cell reorganization time	$1/(\mathrm{Pa} \cdot \mathrm{s})$	1.389×10^{-8}	-

For the latter, we assume a pure hyperelastic behavior with a strain energy

density of the Saint Venant-Kirchhoff type. The remaining values of the parameter are taken equal to those in Table 1 and Table 2.

4 Results

4.1 Growth of a tumor spheroid in vitro

In this section we report the results for a tumor spheroid growing suspended in the culture medium. The radius of the spheroid as a function of time is plotted in Figure 5.a.

Here, the solid line is the result of a numerical simulation where we employed the parameters in Table 1, whereas the dotted markers are experimental data taken from [42]. There is a good agreement with the experimental data, for each of the growth stages of the spheroid. In Figures 7b–7d, we report the evolution of a quantity over the radius of the spheroid for different times during the simulation. In particular, Figure 5.b refers to the mass fraction of oxygen inside the spheroid. Note, at later times, the formation of a nutrient gradient from the spheroid boundary towards its interior. The mass fraction of proliferating tumor cells is shown in Figure 5.c. As the spheroid grows, cell death by necrosis appears at the tumor center, evidenced by zero value of the mass fraction. After 20 days from the beginning of the simulation, a necrotic core is clearly visible. Figure 5.d shows the evolution of the interstitial fluid pressure inside the spheroid. During the first days the tumor increases its radius and, to satisfy the closure relation in (10), the interstitial fluid flows towards the center of the spheroid. As a consequence, the interstitial fluid pressure decreases

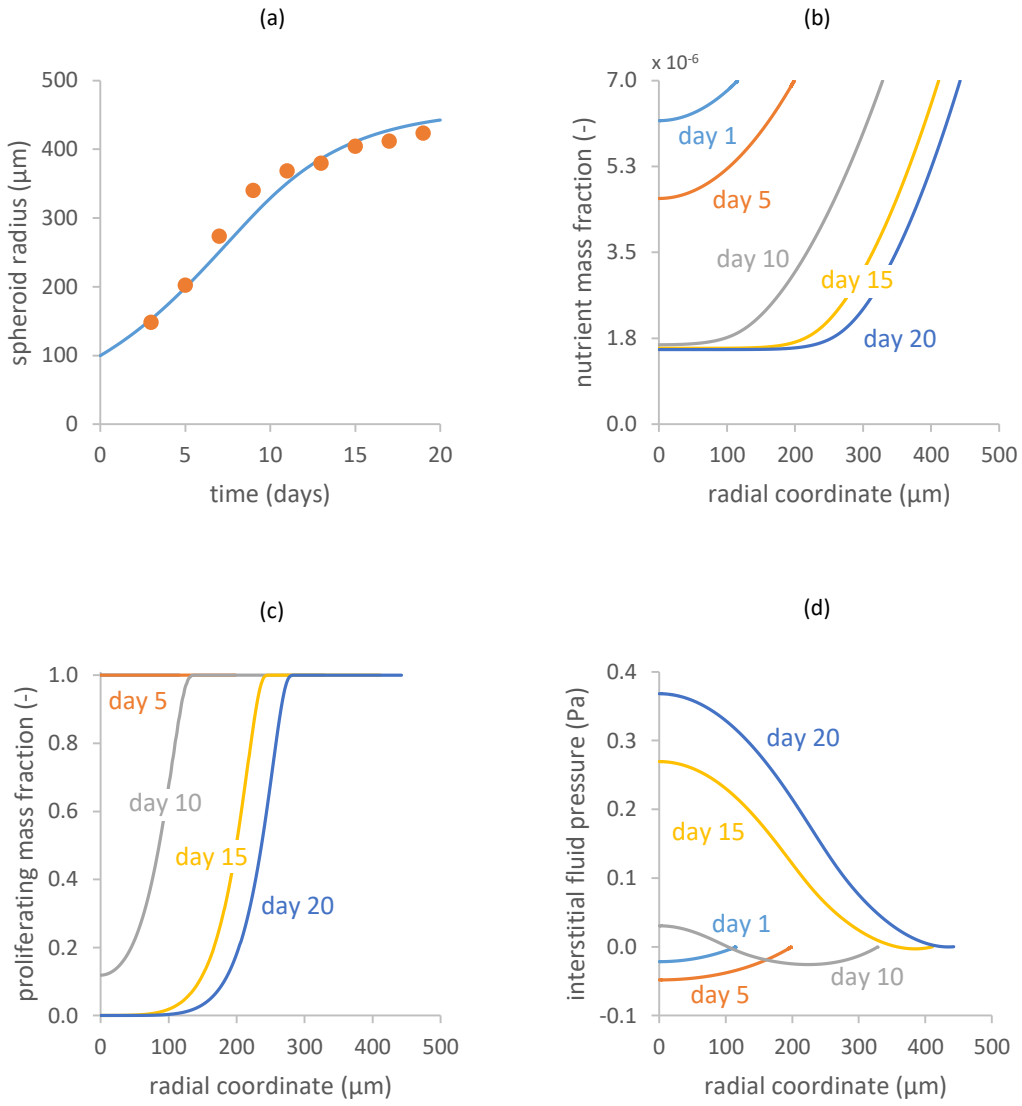

Figure 5: Model results for a tumor spheroid (I). **a** Growth curve of a tumor spheroid (solid line). The dots represent experimental data from [42]. Evolution of the nutrient mass fraction (**b**), the proliferating cell mass fraction (**c**) and the interstitial fluid pressure (**d**) over the radial coordinate and for different times.

within the spheroid center. At later times the interstitial fluid pressure rises inside the tumor, following cell death by lysis. Figure 6 shows a second set of results.

In Figure 6.a, the growth stretch ratio g is plotted at different times. This quantity represents the spherical growth term in the multiplicative decomposition of the deformation gradient. As the tumor mass grows, g increases over the spheroid radius, assuming larger values at the spheroid boundary (where the nutrient level is higher). Note that, after a few days, the value of g decreases within the spheroid center. This is due to a reduction of tumor volume by cell death, and is included in the lysis term of Γ^{s} in equation (7). The evolution of the trace of $\boldsymbol{B}_{\mathrm{p}}$ is reported in Figure 6.b. This quantity measures the plastic distortions occurring in the tumor, which in our framework translate into cell rearrangement. We note that cell rearrangement occurs over the whole spheroid domain, with a peak in the spheroid interior that will be clarified in Figure 7. Then, Figure 6.c shows the variation of the trace of Cauchy stress inside the tumor. As the tumor grows, the portion at the boundary experiences compressive stresses, since $\mathrm{tr}(\boldsymbol{\sigma}^{\mathrm{s}}_{\mathrm{eff}})$ is negative. The situation changes at the tumor interior, where the tissue is subjected to traction and $\mathrm{tr}(\boldsymbol{\sigma}^{\mathrm{s}}_{\mathrm{eff}})$ is positive. Finally, Figure 6.d shows the effective stress of von Mises in the domain. As shown in equation (60), we used this measure of stress to mark the onset of plastic flow. From the graph it is possible to observe that the von Mises stress is constant for the most part of the simulation, maintaining the threshold level imposed by the yield stress. However, after 10 days from the beginning of the simulation, the stress exhibits a peak that is gradually relaxed at later times. This stress peak occurs at the same time as the formation of a necrotic population inside the spheroid, as

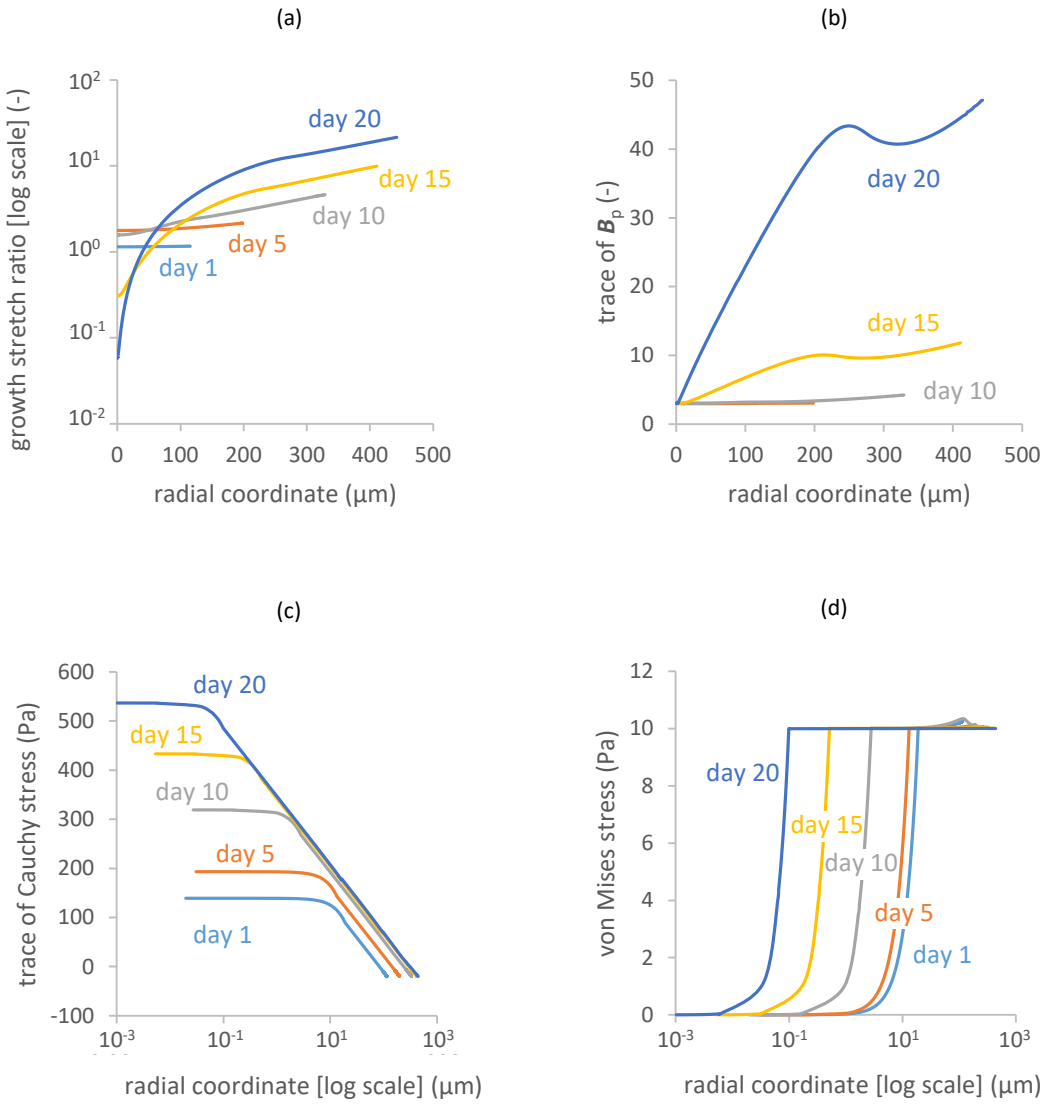

Figure 6: Model results for a tumor spheroid (II). Evolution of the growth stretch ratio (**a**), the trace of $\boldsymbol{B}_\mathrm{p}$ (**b**), the trace of $\boldsymbol{\sigma}^\mathrm{s}_\mathrm{eff}$ (**c**) and the von Mises stress (**d**) over the radial coordinate and for different times.

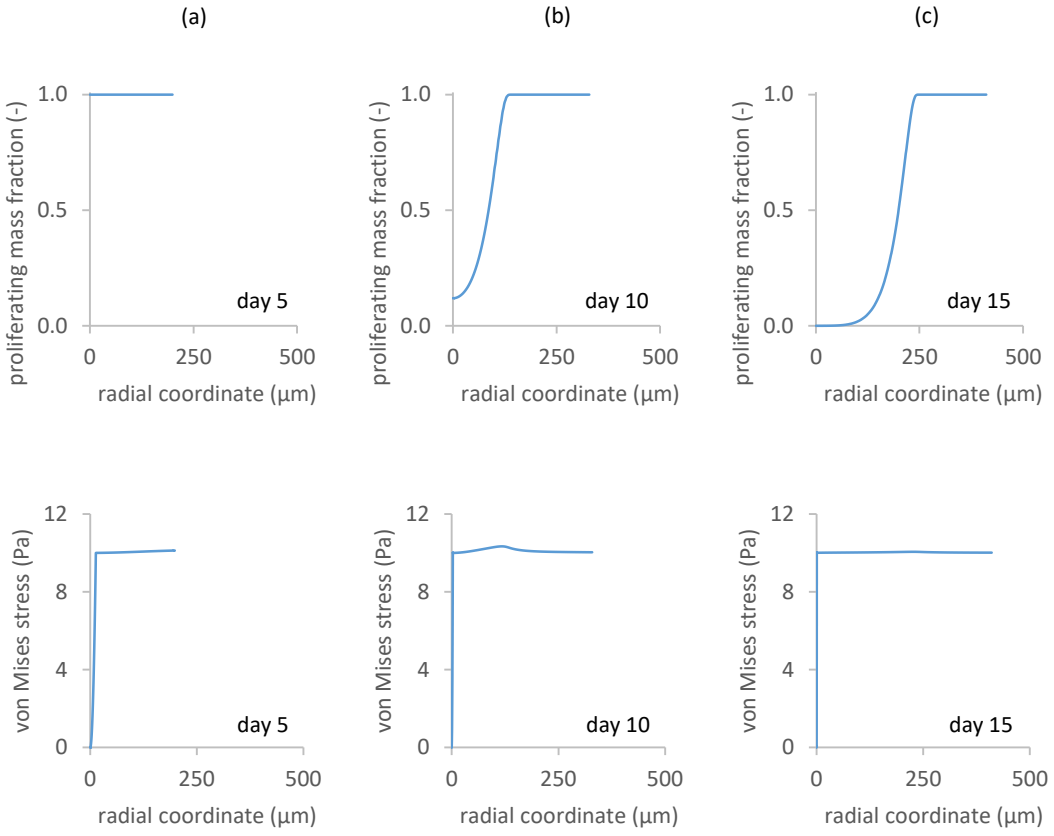

Figure 7: Proliferating cell mass fraction and von Mises stress in the tumor spheroid at different times.

displayed in Figure 7.

Here, the mass fraction of proliferating cells and the von Mises stress are displayed over the radius of the spheroid at day 5 (Figure 7.a), 10 (Figure 7.b) and 15 (Figure 7.c). At day 5, the spheroid is still entirely composed of proliferating cells, and the von Mises stress is relaxing to the yield value. At day 10, however, the oxygen threshold level falls below the critical threshold and a necrotic population is formed at the spheroid core. Interestingly, the peak in von Mises stress is at the

same radial position as the transition between proliferating and necrotic cells. The last snapshot, at day 15, shows an almost completely relaxed state of stress, even if the transition between proliferating and necrotic cells is still present. A possible explanation of the von Mises peak at day 10 could reside in the growth term Γ^{s} of equation (55). The growth stretch ratio decreases in the necrotic region, whereas it increases in the portion of the spheroid in which the cells proliferate. Indeed, in the necrotic region, the mass fraction of the oxygen is lower than the threshold value $\omega^{\mathrm{N}}_{\mathrm{cr}}$, thereby yielding the vanishing of $\Gamma^{\mathrm{p}}_{\mathrm{f}\to\mathrm{p}}$. Consequently, Equation (55) reduces to

$$\frac{\dot{g}}{g} = \frac{\Gamma^{\mathrm{n}}_{\mathrm{n}\to\mathrm{f}}}{3\varphi^{\mathrm{s}}\rho} = -\frac{\gamma^{\mathrm{n}}_{\mathrm{nf}}\omega^{\mathrm{n}}}{3\rho}, \tag{70}$$

and, since all quantities on the right-hand-side of (70) are positive, the time derivative of g is negative. On the other hand, in the proliferating region we have

$$\frac{\dot{g}}{g} = \frac{\Gamma^{\mathrm{p}}_{\mathrm{f}\to\mathrm{p}}}{3\varphi^{\mathrm{s}}\rho} = -\frac{\gamma^{\mathrm{p}}_{\mathrm{fp}}}{3\rho}\left\langle \frac{\omega^{\mathrm{N}} - \omega^{\mathrm{N}}_{\mathrm{cr}}}{\omega^{\mathrm{N}}_{\mathrm{env}} - \omega^{\mathrm{N}}_{\mathrm{cr}}} \right\rangle_{+} \left(1 - \frac{\delta_1 \langle \bar{\sigma}^{\mathrm{s}}_{\mathrm{eff}} \rangle_{+}}{\langle \bar{\sigma}^{\mathrm{s}}_{\mathrm{eff}} \rangle_{+} + \delta_2}\right) \frac{\varphi^{\mathrm{f}}}{\varphi^{\mathrm{f}}_0}\omega^{\mathrm{p}}, \tag{71}$$

yielding, since the oxygen level is above the critical threshold, a positive value for the time derivative of g. This means that the growth stretch ratio is a decreasing or an increasing function of time depending on whether cells are in the necrotic or proliferating region of the spheroid, respectively. According to the picture portrayed by the multiplicative decomposition of the deformation gradient, the elastic distortions evolve to accommodate the growth-induced stresses, and result in the peak occurring in the von Mises stress. Afterwards, this peak is relaxed due to the cell rearrangement, showing the local increase in $\boldsymbol{B}_{\mathrm{p}}$, as visible in Figure 6.b. In the

authors' opinion this result is worth of notice because it is believed to arise from the presence of two species of cells (i.e., the proliferating and the necrotic ones) within a mechanical framework based on the multiplicative decomposition (25), whereas only one cellular species is usually taken into account in this type of models [21, 26, 28, 56]. Further investigations are required to analyze this mechanical response and the possible links to the underlying biology.

4.2 Growth of a tumor in a healthy tissue

To begin our analysis, we first test the model for the case in which plastic rearrangement is turned off in the soft host tissue. These results are shown in Figure 8.

In particular, Figure 8.a represents the evolution of the tumor radius when the tumor is embedded into host tissues of different stiffness. The line marked with "ref." refers to the reference case of a soft host tissue with the mechanical parameters of Table 2. The other lines represent a variation of the parameters μ^h and λ^h of the -75, -50, -25, +25, +50 and +75% with respect to the reference value. As the stiffness of the healthy tissue increases, the final radius of the tumor is reduced. This behavior is similar to the experimental observations of Helmlinger and coworkers [12], where tumor spheroids are grown in gels of different compliances. The other panels of Figure 8 show the evolution of other quantities over the radius of the domain at different times during the simulation. The parameters of Table 2 were used for the healthy tissue, considering the case of no remodeling in the latter. The radial component of the displacement is shown in Figure 8.b. The point of

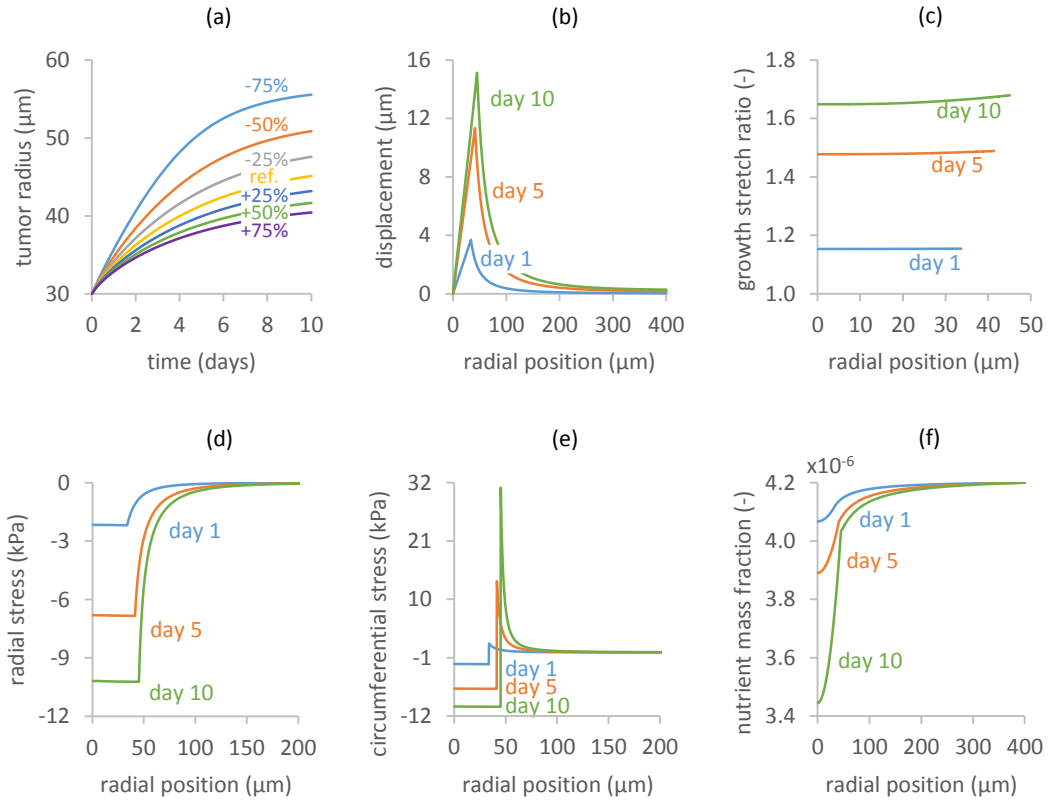

Figure 8: Results for a tumor growing in a soft host tissue (I). **a** Evolution of the tumor radius over time. The different lines range from case of low (-75%) to high (+75%) host tissue stiffness. Variation of the solid displacement (**b**), the growth stretch radius (**c**), the radial stress (**d**), the circumferential stress (**e**) and the nutrient mass fraction (**f**) over the domain radius and for different times.

maximum displacement is at the tumor-host boundary, with a value increasing with time. In accordance to this, the growth stretch ratio (displayed in Figure 8.c) is greater towards the tumor boundary, where a higher concentration of nutrient is available for growth. Then, Figures 8.d and 8.e report the variations in the radial and circumferential stresses, respectively. Note that the two stress components are both compressive and almost uniform in the tumor interior, while at the interface

with the healthy tissue radial stress diminishes and circumferential stress turns to tensile. This result agrees with previous mathematical models investigating the evolution of stress during tumor growth [44, 57, 58]. From the plots it is possible to observe that, even if the yield stress in the tumor is of 10 Pa, the absolute magnitudes of radial and compressive stresses are around a few kPa. This is due to the type of mechanical loading applied on the tumor, which is mainly hydrostatic. Since the flow rule depends on the deviatoric components of the stress, only small plastic deformations are detectable within the tumor domain. Note that the compressive stress applied on the tumor boundary influences also the evolution of the growth stretch ratio in the tumor. In fact, J_e decreases within the tumor as the tissue is compressed. From equation (54), the solid volume fraction in the tumor increases and the porosity decreases accordingly. Since the growth stretch ratio depends on Γ^s and this latter term is linear with respect to porosity (see equation (50)), this results in a reduction of tumor growth. Finally, the evolution of the oxygen mass fraction is shown in Figure 8.f. As the tumor grows, oxygen gradients develop from the periphery to the tumor center. At later times, not reached by the simulation, the oxygen level is expected to fall under the critical threshold, giving rise to a necrotic cell population. The effect of plastic remodeling in the soft host tissue is analyzed in Figure 9.

Dashed lines represent the case where plastic deformation is enabled in the healthy tissue, whereas solid lines refer to the reference case of Figure 8, where remodeling is neglected. For this analysis, we fixed the yield stress in the soft host tissue to be equal to 10^3 Pa and used for the parameters the values in Table 2.

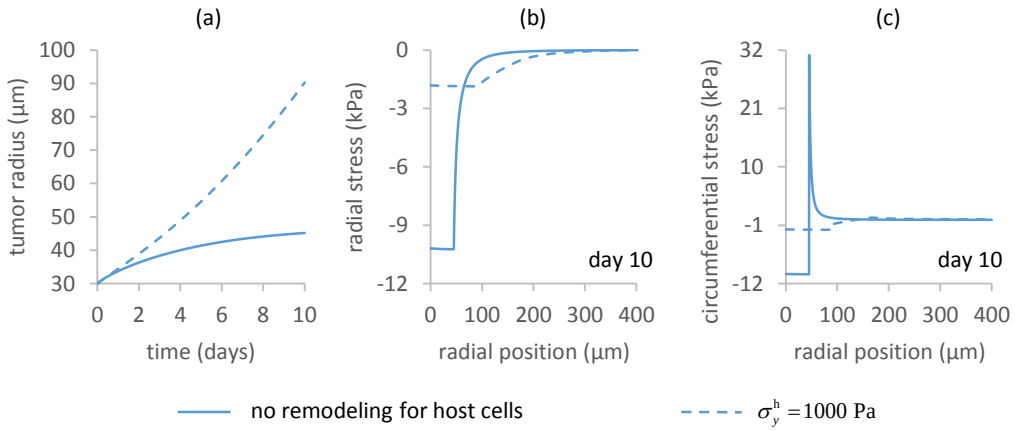

Figure 9: Results for a tumor growing in a soft host tissue (II). Solid or dashed lines represent the cases in which plastic remodeling in the host tissue is neglected or considered, respectively. **a** Evolution of the tumor radius over time. Variation of the radial (**b**) and the circumferential (**c**) stresses over the domain radius and for different times.

The effects of plastic remodeling on the evolution of the tumor radius are shown in Figure 9.a. When compared to the reference case, the tumor grows faster and to a larger extent, reaching a final radius of about 90 μm. This behavior may be explained by considering the effect of stress relaxation induced by plasticity. Indeed, the magnitude of the stresses in the soft host tissue is significantly reduced when compared to the reference case. This is shown in Figure 9.b and Figure 9.c, where the radial and circumferential stresses are plotted over the radius of the domain at the last time-step of the simulation. The steep transitions in the stress between the tumor and soft host tissue are considerably smoothed out and the absolute value of the stress is greatly reduced. Lower mechanical stresses on the tumor boundary constitute a weaker mechanical barrier that may be less able to constrain tumor

growth, leading to larger tumor sizes and host tissue displacements. In addition, as mechanical stress influences cell proliferation through the term in equation (50), smaller compressive stresses provide a minor degree of growth inhibition.

4.3 Tumor growing in the presence of a microvessel and different adjacent tissues

In this section, we investigate the growth of an avascular tumor in a heterogeneous environment. Figure 10.a shows the total displacements at day 7 from the beginning of the simulation.

As the mechanical environment around the tumor is not the same everywhere, the growth of the latter results to be asymmetric. Due to its larger stiffness, the presence of the bone tissue limits the growth of the tumor mass along one direction. Figure 10.b displays the value of the growth stretch ratio over the tumor domain at day 7. Note that the higher values are obtained along the tumor side closer to the capillary surfaces, where there is the maximum value for the nutrient mass fraction. In addition, lower values are displayed over the tumor side that is close to the bone tissue, consistently with Figure 10.a. The nutrient mass fraction at day 7 is shown if Figure 10.c. The lowest values are attained at the tumor center, where nutrient consumption is more pronounced. Finally, Figure 10.d shows the trace of $\boldsymbol{B}_{\mathrm{p}}$ at day 7 over the tissue external to the tumor. The area close to the tumor boundary is subjected to the higher plastic remodeling. As the tumor expands, the healthy tissue is displaced from its original position and the host cells need to rearrange their relative bonds to accommodate the new configuration. The asymmetric tumor

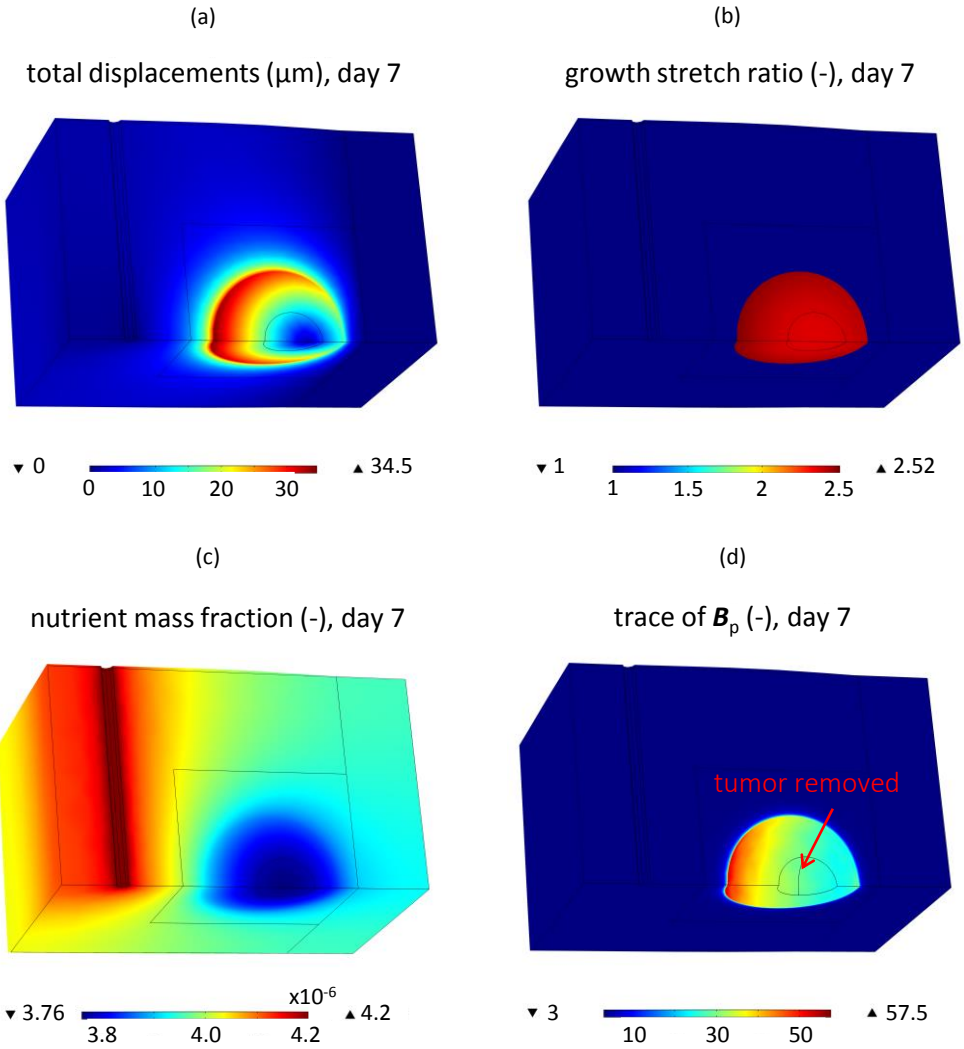

Figure 10: Results for an avascular tumor growing in a heterogeneous environment. The solid displacements (**a**), the growth stretch ratio (**b**), the nutrient mass fraction (**c**) and the trace of $\boldsymbol{B}_{\mathrm{p}}$ (**d**) are plotted over the three-dimensional domain at the end of the simulation.

growth pattern is highlighted in Figure 11, where we display the lateral displacement of the tumor points shown in the inset. The two curves gradually diverge, showing a different evolution over time of the growth rate for the points.

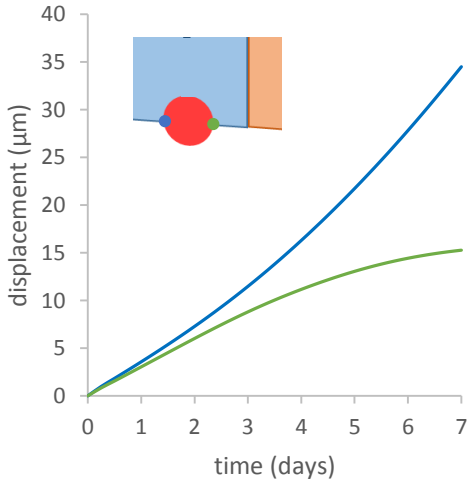

Figure 11: Growth curves of two different points in the tumor.

5 Conclusions

In the present study, a mathematical model for avascular tumor growth is presented. The modeling framework is based on porous media mechanics and the concept of evolving natural configurations, extending previous works in the literature. We start by considering the growth of a tumor spheroid, where proliferating tumor cells undergo necrosis if subjected to low levels of nutrient. We analyze the evolution of different quantities, such as the growth stretch ratio, oxygen mass fraction and mechanical stresses, over the spheroid radius for different times. Then, we evaluate the effect of stress relaxation induced by cell reorganization in the spheroid. Interestingly, when proliferating cells become necrotic, we observe a peak in the von Mises equivalent stress, followed by a progressive relaxation induced by the plastic contribution to the deformation gradient. After that, we study the growth of a spherical tumor embedded into a healthy tissue. We consider the effects of different mechan-

ical properties of the latter on the tumor. In particular, we vary the external tissue stiffness and we consider both the case of no remodeling and active remodeling in the soft host tissue. We analyze the effect of these features on the tumor radius and on the radial and circumferential stresses inside the domain. We observe the influence of plastic reorganization on the soft host tissue, and we note that the tumor grows larger in a soft host tissue where remodeling is enabled. Finally, we consider the case of a tumor grown in a host tissue made of two distinct compartments, i.e. a healthy soft tissue and a bone. The different mechanical properties of the two tissues affect significantly the growth of the tumor mass, which, starting from a spherical form, assumes an asymmetric shape at the end of the simulation. Since one of the two domains is stiffer than the other, and since the cancer cells proliferate more towards the region of least mechanical resistance, the tumor extends more in the softer host tissue.

Several simplifying assumptions are considered in the study, and the work is certainly open to further improvements. The modeling framework is simplified with respect to the more general model of [59], in which tumor cells and host cells are treated as fluids. In fact, the present model does not allow to take into account migration of cells through the ECM [60]; possible detachment of the cells from the ECM and from other cell populations; different stiffness of the cell population with respect to the ECM (with which they are here lumped); build-up of cortical tension between healthy and tumor tissues; and possible invasion of the tumor tissue by the healthy tissue or vice versa, mediated by these cortical tensions. It allows, however, for displacement of the host tissue by the tumor and also investigation of

possible fingering. For the future, we are planning to develop the model proposed here by taking into account different phenomena. In particular, the adhesion mechanisms between the cells and the ECM should be investigated in more detail. This will probably lead to a modification of the plastic flow rule, including the effect of different adhesion molecules, such as catherins and integrins. Moreover, cells belonging to distinct cellular populations should display different adhesive characteristics, leading to a modified expression for the yield stress. Model development requires experiments that are able to provide better estimates for the model parameters. Furthermore, new sets of data in terms of quantities that can be compared to the output of the model equations are needed. Part of the future experimental work should also be devoted to supply measures of the yield stress, with experiments like those in [51, 50, 61]. To this regard, it would be extremely interesting to investigate the mechanical response of tumor spheroids subjected to both compressive and shear stresses, also interfering with the adhesion molecules by using different drugs.

Describing more thoroughly the interactions between the tumor and its external microenvironment (both biochemical and mechanical) should offer valuable insight into the understanding of the disease progression, with the final aim of helping the design of new therapeutic treatments.

Acknowledgments

PM, MC and AC have been partially financed by the *Politecnico di Torino* and the *Fondazione Cassa di Risparmio di Torino* in the context of the funding campaign *"La Ricerca dei Talenti"* (HR Excellence in Research). BAS acknowledges the sup-

port of the Technische Universität München - Institute for Advanced Study, funded by the German Excellence Initiative and the European Union Seventh Framework Programme under grant agreement n° 291763. The authors thank Prof. Luigi Preziosi for critical reading of the manuscript and for helpful discussions.

Declaration of Conflicting Interests

The Authors declare that there is no conflict of interest.

Appendix A

We derive the material form of the equations (55)-(58).

Starting from (4), for the mass balance equation of the solid phase we write:

$$\mathcal{D}^{\mathrm{s}}\left(\varphi^{\mathrm{s}}\rho^{\mathrm{s}}\right)+\varphi^{\mathrm{s}}\rho^{\mathrm{s}}\mathrm{div}\left(\boldsymbol{v}^{\mathrm{s}}\right)=\Gamma^{\mathrm{s}}, \tag{72}$$

where $\mathcal{D}^{\mathrm{s}}\left(\cdot\right)=\partial_t\left(\cdot\right)+\boldsymbol{v}^{\mathrm{s}}\cdot\mathrm{grad}\,\left(\cdot\right)$ denotes the material derivative of the argument. From the identity $\dot{J}=J\mathrm{div}\left(\boldsymbol{v}^{\mathrm{s}}\right)$ we can write in the reference configuration:

$$\dot{\overline{\varphi^{\mathrm{s}}\rho^{\mathrm{s}}}}+\varphi^{\mathrm{s}}\rho^{\mathrm{s}}\frac{\dot{J}}{J}=\Gamma^{\mathrm{s}}, \tag{73}$$

$$\dot{\overline{J\varphi^{\mathrm{s}}\rho^{\mathrm{s}}}}=\dot{\overline{J_{\mathrm{e}}\varphi^{\mathrm{s}}\rho^{\mathrm{s}}}}J_{\mathrm{g}}+J_{\mathrm{e}}\varphi^{\mathrm{s}}\rho^{\mathrm{s}}\dot{J}_g=\dot{\overline{J_{\mathrm{e}}\varphi^{\mathrm{s}}\rho^{\mathrm{s}}}}J_{\mathrm{g}}+3J\varphi^{\mathrm{s}}\rho^{\mathrm{s}}\frac{\dot{g}}{g}=J\Gamma^{\mathrm{s}}, \tag{74}$$

with $\dot{J}_{\mathrm{g}}=J_{\mathrm{g}}\mathrm{tr}\left(\dot{\boldsymbol{F}}_{\mathrm{g}}\boldsymbol{F}_{\mathrm{g}}^{-1}\right)=3J_{\mathrm{g}}\,\dot{g}/g$. If we impose that the rate of change of mass

contributes entirely to the growth term, then we have:

$$\varphi^{\mathrm{s}}\rho^{\mathrm{s}}J_{\mathrm{e}} = \rho_0^{\mathrm{s}} = \text{const.} \tag{75}$$

and equation (74) gives:

$$\frac{\dot{g}}{g} = \frac{1}{3}\frac{\Gamma^{\mathrm{s}}}{\varphi^{\mathrm{s}}\rho^{\mathrm{s}}}, \tag{76}$$

whereas equation (75) gives an expression for φ^{s}:

$$\varphi^{\mathrm{s}} = \frac{\rho_0^{\mathrm{s}}}{\rho^{\mathrm{s}}J_{\mathrm{e}}} = \frac{g^3\rho_0^{\mathrm{s}}}{\rho^{\mathrm{s}}J}, \tag{77}$$

and we also have that:

$$\varphi_\nu^{\mathrm{s}} = \varphi^{\mathrm{s}}J_{\mathrm{e}} = \frac{\rho_0^{\mathrm{s}}}{\rho^{\mathrm{s}}}. \tag{78}$$

Note that, in general, ρ^{s} can depend on the mass fraction of the constituents, i.e. $\rho^{\mathrm{s}} = \rho^{\mathrm{s}}\left(\omega^{\mathrm{p}}, \omega^{\mathrm{n}}\right)$.

The mass balance equation for the proliferating cells reads

$$\mathcal{D}^{\mathrm{s}}\left(\varphi^{\mathrm{s}}\rho^{\mathrm{s}}\omega^{\mathrm{p}}\right) + \varphi^{\mathrm{s}}\rho^{\mathrm{s}}\omega^{\mathrm{p}}\mathrm{div}\left(\boldsymbol{v}^{\mathrm{s}}\right) = \Gamma^{\mathrm{p}}_{\mathrm{p}\to\mathrm{n}} + \Gamma^{\mathrm{p}}_{\mathrm{f}\to\mathrm{p}}, \tag{79}$$

$$\overset{\cdot}{\overline{\varphi^{\mathrm{s}}\rho^{\mathrm{s}}\omega^{\mathrm{p}}J}} = J\Gamma^{\mathrm{s}}\omega^{\mathrm{p}} + J\varphi^{\mathrm{s}}\rho^{\mathrm{s}}\dot{\omega}^{\mathrm{p}} = J\left(\Gamma^{\mathrm{p}}_{\mathrm{p}\to\mathrm{n}} + \Gamma^{\mathrm{p}}_{\mathrm{f}\to\mathrm{p}}\right), \tag{80}$$

$$\dot{\omega}^{\mathrm{p}} = \frac{J}{\rho_0^{\mathrm{s}}g^3}\left(\Gamma^{\mathrm{p}}_{\mathrm{p}\to\mathrm{n}} + \Gamma^{\mathrm{p}}_{\mathrm{f}\to\mathrm{p}} - \omega^{\mathrm{p}}\Gamma^{\mathrm{s}}\right) = \frac{1}{\varphi^{\mathrm{s}}\rho^{\mathrm{s}}}\left(\Gamma^{\mathrm{p}}_{\mathrm{p}\to\mathrm{n}} + \Gamma^{\mathrm{p}}_{\mathrm{f}\to\mathrm{p}} - \omega^{\mathrm{p}}\Gamma^{\mathrm{s}}\right), \tag{81}$$

in which equations (75) and (76) are used. Similarly, for the necrotic portion of the cells we can write:

$$\dot{\omega}^{\mathrm{n}} = \frac{J}{\rho_0^{\mathrm{s}}g^3}\left(\Gamma^{\mathrm{n}}_{\mathrm{n}\to\mathrm{f}} + \Gamma^{\mathrm{n}}_{\mathrm{p}\to\mathrm{n}} - \omega^{\mathrm{n}}\Gamma^{\mathrm{s}}\right). \tag{82}$$

The mass balance equation for the whole solid-fluid system is obtained by summing up the two mass balance equations for the solid and the fluid phase, which read

$$\partial_t \varphi^{\mathrm{s}} + \operatorname{div}\left(\varphi^{\mathrm{s}} \boldsymbol{v}^{\mathrm{s}}\right) + \frac{\varphi^{\mathrm{s}}}{\rho^{\mathrm{s}}} \mathcal{D}^{\mathrm{s}} \rho^{\mathrm{s}} = \frac{\Gamma^{\mathrm{s}}}{\rho^{\mathrm{s}}}, \tag{83}$$

$$\partial_t \varphi^{\mathrm{f}} + \operatorname{div}\left(\varphi^{\mathrm{f}} \boldsymbol{v}^{\mathrm{f}}\right) + \frac{\varphi^{\mathrm{f}}}{\rho^{\mathrm{f}}} \mathcal{D}^{\mathrm{f}} \rho^{\mathrm{f}} = -\frac{\Gamma^{\mathrm{s}}}{\rho^{\mathrm{f}}}, \tag{84}$$

respectively. Summing equation (83) and (84) gives:

$$\operatorname{div}\left(\boldsymbol{q}\right) + \operatorname{div}\left(\boldsymbol{v}^{\mathrm{s}}\right) + \varphi^{\mathrm{f}} \beta^{\mathrm{f}} + \varphi^{\mathrm{s}} \beta^{\mathrm{s}} = \left(\frac{1}{\rho^{\mathrm{s}}} - \frac{1}{\rho^{\mathrm{f}}}\right) \Gamma^{\mathrm{s}}, \tag{85}$$

in which $\beta^{\mathrm{j}} = \mathcal{D}^{\mathrm{j}} \rho^{\mathrm{j}} / \rho^{\mathrm{j}}$, $\mathrm{j} = \mathrm{f}, \mathrm{s}$ represent the compressibility of the j-th phase, and $\boldsymbol{q} = \varphi^{\mathrm{f}} \left(\boldsymbol{v}^{\mathrm{f}} - \boldsymbol{v}^{\mathrm{s}}\right)$. Note that

$$\varphi^{\mathrm{f}} \beta^{\mathrm{f}} = \frac{\varphi^{\mathrm{f}}}{\rho^{\mathrm{f}}} \left[\mathcal{D}^{\mathrm{s}} \rho^{\mathrm{f}} + \left(\boldsymbol{v}^{\mathrm{f}} - \boldsymbol{v}^{\mathrm{s}}\right) \cdot \operatorname{grad} \rho^{\mathrm{f}}\right] = \varphi^{\mathrm{f}} \frac{\mathcal{D}^{\mathrm{s}} \rho^{\mathrm{f}}}{\rho^{\mathrm{f}}} + \frac{\operatorname{grad} \rho^{\mathrm{f}} \cdot \boldsymbol{q}}{\rho^{\mathrm{f}}}. \tag{86}$$

By employing (86) and applying a Piola Transformation of equation (85) we obtain

$$\operatorname{Div}\left(\boldsymbol{Q}\right) + \dot{J} + J\left(1 - \varphi^{\mathrm{s}}\right) \frac{\dot{\rho}^{\mathrm{f}}}{\rho^{\mathrm{f}}} + \frac{1}{\rho^{\mathrm{f}}} \boldsymbol{Q} \cdot \operatorname{Grad} \rho^{\mathrm{f}} + J \varphi^{\mathrm{s}} \frac{\dot{\rho}^{\mathrm{s}}}{\rho^{\mathrm{s}}} = J \left(\frac{1}{\rho^{\mathrm{s}}} - \frac{1}{\rho^{\mathrm{f}}}\right) \Gamma^{\mathrm{s}}, \tag{87}$$

where we defined $\boldsymbol{Q} = J \boldsymbol{F}^{-1} \boldsymbol{q}$. Note that if the densities of the phases are assumed to be constant and equal to each other the expression above can be simplified into:

$$\operatorname{Div}\left(\boldsymbol{Q}\right) + \dot{J} = 0, \tag{88}$$

with $\boldsymbol{Q}$ given as:

$$\boldsymbol{Q} = -J\boldsymbol{F}^{-1}\boldsymbol{k}\boldsymbol{F}^{-T}\text{Grad } p^{\text{f}}. \tag{89}$$

Here $\boldsymbol{k}$ is the hydraulic conductivity tensor of the solid.

For the nutrient species we rewrite the mass balance equation as:

$$\mathcal{D}^{\text{s}}\left(\varphi^{\text{f}}\rho^{\text{f}}\omega^{\text{N}}\right) + \varphi^{\text{f}}\rho^{\text{f}}\omega^{\text{N}}\text{div}\left(\boldsymbol{v}^{\text{s}}\right) + \text{div}\left[\varphi^{\text{f}}\rho^{\text{f}}\omega^{\text{N}}\left(\boldsymbol{v}^{\text{f}} - \boldsymbol{v}^{\text{s}}\right) + \boldsymbol{J}^{\text{N}}\right] = \Gamma^{\text{N}}_{\text{N}\to\text{p}}, \tag{90}$$

where $\boldsymbol{J}^{\text{N}} = -\varphi^{\text{f}}\rho^{\text{f}}\boldsymbol{D}^{\text{N}}\text{grad}\,\omega^{\text{N}}$. The term $\boldsymbol{D}^{\text{N}}$ is the diffusivity tensor of the nutrient dissolved into the interstitial fluid. This equation can be rewritten in the material frame as:

$$\dot{\overline{J\varphi^{\text{f}}\rho^{\text{f}}\omega^{\text{N}}}} + \text{Div}\left(\rho^{\text{f}}\omega^{\text{N}}\boldsymbol{Q} + \boldsymbol{\Psi}^{\text{N}}\right) = J\Gamma^{\text{N}}_{\text{N}\to\text{p}}, \tag{91}$$

where the material diffusive flux is written as $\boldsymbol{\Psi}^{\text{N}} = -J\varphi^{\text{f}}\rho^{\text{f}}\boldsymbol{F}^{-1}\boldsymbol{D}^{\text{N}}\boldsymbol{F}^{-T}\text{Grad}\,\omega^{\text{N}}$. By manipulating this equation, and knowing that

$$\mathcal{D}^{\text{f}}\left(\varphi^{\text{f}}\rho^{\text{f}}\right) + \varphi^{\text{f}}\rho^{\text{f}}\text{div}\left(\boldsymbol{v}^{\text{f}}\right) = \Gamma^{\text{f}}, \tag{92}$$

$$\mathcal{D}^{\text{s}}\left(\varphi^{\text{f}}\rho^{\text{f}}\right) + \text{div}\left(\rho^{\text{f}}\varphi^{\text{f}}\boldsymbol{q}\right) + \varphi^{\text{f}}\rho^{\text{f}}\text{div}\left(\boldsymbol{v}^{\text{s}}\right) = -\Gamma^{\text{s}}, \tag{93}$$

$$\dot{\overline{J\varphi^{\text{f}}\rho^{\text{f}}}} + \text{Div}\left(\rho^{\text{f}}\boldsymbol{Q}\right) = -J\Gamma^{\text{s}}, \tag{94}$$

we arrive at the final form of the nutrient mass balance equation, which reads

$$J\varphi^{\text{f}}\rho^{\text{f}}\dot{\omega}^{\text{N}} + \rho^{\text{f}}\boldsymbol{Q}\cdot\text{Grad}\,\omega^{\text{N}} + \text{Div}\left(\boldsymbol{\Psi}^{\text{N}}\right) = J\left(\Gamma^{\text{N}}_{\text{N}\to\text{p}} + \omega^{\text{N}}\Gamma^{\text{s}}\right). \tag{95}$$

References

[1] Weinberg R. *The Biology of Cancer, Second Edition.* Taylor & Francis Group, 2013. ISBN 9781317963462.

[2] Longo D, Fauci A, Kasper D et al. *Harrison's Principles of Internal Medicine, 18th Edition.* McGraw-Hill Education, 2011. ISBN 9780071748902.

[3] Alberts B. *Molecular Biology of the Cell: Reference edition.* Molecular Biology of the Cell: Reference Edition, Garland Science, 2008. ISBN 9780815341116.

[4] Thompson DAW. *On Growth and Form.* Dover Books on Biology Series, Dover, 1942. ISBN 9780486671352.

[5] Taber LA. Biomechanics of growth, remodeling, and morphogenesis. *Appl Mech Rev* 1995; 48(8): 487.

[6] Heller E and Fuchs E. Tissue patterning and cellular mechanics. *J Cell Biol* 2015; 211(2): 219–31.

[7] Risler T. Focus on the physics of cancer. *New J Phys* 2015; 17(5): 055011.

[8] Mueller-Klieser W. Tumor biology and experimental therapeutics. *Crit Rev Oncol Hematol* 2000; 36(2-3): 123–39.

[9] Vander Heiden MG, Cantley LC and Thompson CB. Understanding the Warburg effect: the metabolic requirements of cell proliferation. *Science* 2009; 324(5930): 1029–33.

[10] Lee DA, Knight MM, Campbell JJ et al. Stem cell mechanobiology. *J Cell Biochem* 2011; 112(1): 1–9.

[11] Frank V et al. Frequent mechanical stress suppresses proliferation of mesenchymal stem cells from human bone marrow without loss of multipotency. *Sci Rep* 2016; 6(April): 24264.

[12] Helmlinger G, Netti PA, Lichtenbeld HC et al. Solid stress inhibits the growth of multicellular tumor spheroids. *Nat Biotechnol* 1997; 15(8): 778–83.

[13] Cheng G, Tse J, Jain RK et al. Micro-environmental mechanical stress controls tumor spheroid size and morphology by suppressing proliferation and inducing apoptosis in cancer cells. *PLOS ONE* 2009; 4(2): e4632.

[14] Desmaison A, Frongia C, Grenier K et al. Mechanical stress impairs mitosis progression in multi-cellular tumor spheroids. *PLOS ONE* 2013; 8(12): e80447.

[15] Montel F et al. Stress clamp experiments on multicellular tumor spheroids. *Phys Rev Lett* 2011; 107(18): 188102.

[16] Hanahan D and Weinberg RA. The hallmarks of cancer. *Cell* 2000; 100(1): 57–70.

[17] Hanahan D and Weinberg RA. Hallmarks of cancer: the next generation. *Cell* 2011; 144(5): 646–74.

[18] Ambrosi D, Preziosi L and Vitale G. The interplay between stress and growth in solid tumors. *Mech Res Commun* 2012; 42: 87–91.

[19] Sciumè G, Gray WG, Ferrari M et al. On computational modeling in tumor growth. *Arch Comput Meth Eng* 2013; 20(4): 327–352.

[20] Skalak R. Growth as a finite displacement field. In *Proceedings of the IUTAM Symposium on Finite Elasticity*. Springer Netherlands. ISBN 978-94-009-7540-8, pp. 347–355.

[21] Rodriguez EK, Hoger A and McCulloch AD. Stress-dependent finite growth in soft elastic tissues. *J Biomech* 1994; 27(4): 455–67.

[22] Bilby AB, Gardner LRT and Stroh AN. Continuous distributions of dislocations and the theory of plasticity. In *Proceedings of the XIth ICTAM*. Presses de l'Université of Bruxelles.

[23] Kröner E. Allgemeine Kontinuumstheorie der Versetzungen und Eigenspannungen. *Arch Rational Mech Anal* 1959; 4: 273.

[24] Lee EH. Elastic-plastic deformation at finite strains. *J Appl Mech* 1969; 36: 1–6.

[25] Humphrey JD and Rajagopal KR. A constrained mixture model for growth and remodeling of soft tissues. *Math Mod Meth Appl S* 2002; 12(03): 407–430.

[26] Ambrosi D and Mollica F. On the mechanics of a growing tumor. *Int J Eng Sci* 2002; 40(12): 1297–1316.

[27] Ambrosi D and Mollica F. The role of stress in the growth of a multicell spheroid. *J Math Biol* 2004; 48(5): 477–499.

[28] Ambrosi D and Preziosi L. Cell adhesion mechanisms and stress relaxation in the mechanics of tumours. *Biomech Model Mechanobiol* 2009; 8(5): 397–413.

[29] Preziosi L, Ambrosi D and Verdier C. An elasto-visco-plastic model of cell aggregates. *J Theor Biol* 2010; 262(1): 35–47.

[30] Giverso C and Preziosi L. Modelling the compression and reorganization of cell aggregates. *Math Med Biol* 2012; 29: 181–204.

[31] Giverso C and Preziosi L. Behavior of cell aggregates under force-controlled compression. *Int J Non Linear Mech* 2013; 56: 50–55.

[32] Giverso C, Scianna M and Grillo A. Growing avascular tumours as elasto-plastic bodies by the theory of evolving natural configurations. *Mech Res Commun* 2015; 68: 31–39.

[33] Hassanizadeh SM. Derivation of basic equations of mass transport in porous media, part 2. generalized darcy's and fick's laws. *Adv Water Res* 1986; 9(4): 207 – 222.

[34] Lewis RW and Schrefler BA. *The Finite Element Method in the Static and Dynamic Deformation and Consolidation of Porous Media*. Numerical methods in engineering, John Wiley, 1998. ISBN 9780471928096.

[35] Epstein M and Maugin GA. Thermomechanics of volumetric growth in uniform bodies. *Int J Plasticity* 2000; 16(7): 951–978.

[36] Mićunović MV. *Thermomechanics of ViscoplasticityFundamentals and Applications*. Springer-Verlag New York, 2009. ISBN 978-0-387-89489-8.

[37] Grillo A, Prohl R and Wittum G. A generalised algorithm for anelastic processes in elastoplasticity and biomechanics. *Math Mech Solids* 2015; : doi:10.1177/1081286515598661.

[38] Holmes MH and Mow VC. The nonlinear characteristics of soft gels and hydrated connective tissues in ultrafiltration. *J Biomech* 1990; 23(11): 1145–56.

[39] Grillo A, Prohl R and Wittum G. A poroplastic model of structural reorganisation in porous media of biomechanical interest. *Continuum Mech Therm* 2016; 28(1-2): 579–601.

[40] Maugin GA and Epstein M. Geometrical material structure of elastoplasticity. *Int J Plasticity* 1998; 14(1-3): 109–115.

[41] Simo J and Hughes T. *Computational Inelasticity*. Interdisciplinary Applied Mathematics, Springer-Verlag New York, 1998. ISBN 978-1-4757-7169-5.

[42] Mascheroni P, Stigliano C, Carfagna M et al. Predicting the growth of glioblastoma multiforme spheroids using a multiphase porous media model. *Biomech Model Mechanobiol* 2016; 15(5): 1215–28.

[43] Sciumè G, Shelton S, Gray WG et al. A multiphase model for three-dimensional tumor growth. *New J Phys* 2013; 15(1): 015005.

[44] Roose T, Netti Pa, Munn LL et al. Solid stress generated by spheroid growth estimated using a linear poroelasticity model. *Microvasc Res* 2003; 66(3): 204–212.

[45] Mueller-Klieser WF and Sutherland RM. Oxygen tensions in multicell spheroids of two cell lines. *Br J Cancer* 1982; 45(2): 256–264.

[46] Mueller-Klieser W, Freyer JP and Sutherland RM. Influence of glucose and oxygen supply conditions on the oxygenation of multicellular spheroids. *Br J Cancer* 1986; 53(3): 345–53.

[47] Casciari JJ, Sotirchos SV and Sutherland RM. Mathematical modelling of microenvironment and growth in EMT6/Ro multicellular tumour spheroids. *Cell Prolif* 1992; 25(1): 1–22.

[48] Casciari JJ, Sotirchos SV and Sutherland RM. Variations in tumor cell growth rates and metabolism with oxygen concentration, glucose concentration, and extracellular pH. *J Cell Physio* 1992; 151(2): 386–94.

[49] Gaspar N, Sharp SY, Pacey S et al. Acquired resistance to 17-allylamino-17-demethoxygeldanamycin (17-AAG, tanespimycin) in glioblastoma cells. *Cancer Res* 2009; 69(5): 1966–75.

[50] Forgacs G, Foty Ra, Shafrir Y et al. Viscoelastic properties of living embryonic tissues: a quantitative study. *Biophys J* 1998; 74(5): 2227–34.

[51] Iordan A, Duperray A and Verdier C. Fractal approach to the rheology of concentrated cell suspensions. *Phys Rev E* 2008; 77(1 Pt 1): 011911.

[52] Mpekris F, Angeli S, Pirentis AP et al. Stress-mediated progression of solid tumors: effect of mechanical stress on tissue oxygenation, cancer cell proliferation, and drug delivery. *Biomech Model Mechanobiol* 2015; 14(6): 1391–402.

[53] Frieboes HB, Zheng X, Sun CH et al. An integrated computational/experimental model of tumor invasion. *Cancer Res* 2006; 66(3): 1597–604.

[54] Lacroix D and Prendergast PJ. A mechano-regulation model for tissue differentiation during fracture healing: analysis of gap size and loading. *J Biomech* 2002; 35(9): 1163–71.

[55] Kelly DJ and Prendergast PJ. Mechano-regulation of stem cell differentiation and tissue regeneration in osteochondral defects. *J Biomech* 2005; 38(7): 1413–22.

[56] Stylianopoulos T, Martin JD, Snuderl M et al. Coevolution of solid stress and interstitial fluid pressure in tumors during progression: implications for vascular collapse. *Cancer Res* 2013; 73(13): 3833–41.

[57] Sarntinoranont M, Rooney F and Ferrari M. Interstitial stress and fluid pressure within a growing tumor. *Ann Biomed Eng* 2003; 31(3): 327–35.

[58] Voutouri C, Mpekris F, Papageorgis P et al. Role of constitutive behavior and tumor-host mechanical interactions in the state of stress and growth of solid tumors. *PLOS ONE* 2014; 9(8): e104717.

[59] Sciumè G, Santagiuliana R, Ferrari M et al. A tumor growth model with deformable ECM. *Phys Biol* 2014; 11(6): 65004.

[60] Sciumè G, Gray WG, Hussain F et al. Three phase flow dynamics in tumor growth. *Comput Mech* 2013; 53(3): 465–484.

[61] Marmottant P, Mgharbel A, Kafer J et al. The role of fluctuations and stress on the effective viscosity of cell aggregates. *Proc Natl Acad Sci* 2009; 106(41): 17271–17275.